Published in final edited form as:

Cytokine. 2022 December ; 160: 156022. doi:10.1016/j.cyto.2022.156022.

Histopathologic and Transcriptomic Phenotypes of a Conditional RANKL Transgenic Mouse Thymus

Maria M. Szwarc[a,1], **Lan Hai**[a,1], **Vineet K. Maurya**[a], **Kimal Rajapakshe**[a], **Dimuthu Perera**[a], **Michael M. Ittmann**[b], **Qianxing Mo**[c], **Yong Lin**[d], **Matthew L. Bettini**[d], **Cristian Coarfa**[a,2], **John P. Lydon**[a,*]

[a]Department of Molecular & Cellular Biology, Baylor College of Medicine, Houston, Texas

[b]Department of Pathology, Baylor College of Medicine, Houston, Texas

[c]Department of Biostatistics & Bioinformatics, H. Lee Moffitt Cancer Center & Research Institute, Tampa, Florida

[d]Department of Pathology, University of Utah School of Medicine, Salt Lake City, Utah

Abstract

Although conventional knockout and transgenic mouse models have significantly advanced our understanding of Receptor Activator of NF-κB Ligand (RANKL) signaling in intra-thymic crosstalk that establishes self-tolerance and later stages of lymphopoiesis, the unique advantages of conditional mouse transgenesis have yet to be explored. A main advantage of conditional transgenesis is the ability to express a transgene in a spatiotemporal restricted manner, enabling the induction (or de-induction) of transgene expression during predetermined stages of embryogenesis or during defined postnatal developmental or physiological states, such as puberty, adulthood, and pregnancy. Here, we describe the *K5: RANKL* bigenic mouse, in which transgene derived RANKL expression is induced by doxycycline and targeted to cytokeratin 5 positive medullary thymic epithelial cells (mTECs). Short-term doxycycline induction reveals that RANKL transgene expression is significantly induced in the thymic medulla and only in response to doxycycline. Prolonged doxycycline induction in the *K5: RANKL* bigenic results in a significantly enlarged thymus in which mTECs are hyperproliferative. Flow cytometry showed that there is a marked enrichment of CD4+ and CD8+ single positive thymocytes with a concomitant depletion of CD4+CD8+ double positives. Furthermore, there is an increase in the number of FOXP3+ T regulatory (Treg) cells and Ulex Europaeus Agglutinin 1+ (UEA1+) mTECs. Transcriptomics revealed that a remarkable array of signals—cytokines, chemokines, growth factors, transcription factors, and morphogens—are governed by RANKL and drive in part

*Corresponding author: jlydon@bcm.edu (J.P. Lydon). [2]Co-corresponding author.
[1]Equal contribution (co-first authors)

Authors' contributions

MMS, LH, VKM, and JPL designed and/or conducted the experiments described in the manuscript. YL and MLB performed the flow cytometry studies. QM, KR, DP, and CC were involved in various aspects of the bioinformatic analyses. MMS conducted the end-stage pathway analysis of the RNA-seq datasets. Histopathology evaluations were conducted by MMI and JPL. The studies were overseen by JPL while most of the manuscript and figures were prepared by MMS, LH, VKM, and JPL. All authors reviewed and approved the final draft of the manuscript.

Declaration of Competing Interest

The authors declare that they have no conflict of interest concerning the studies described herein.

the *K5: RANKL* thymic phenotype. Extended doxycycline administration to 6-weeks results in a *K5: RANKL* thymus that begins to display distinct histopathological features, such as medullary epithelial hyperplasia, extensive immune cell infiltration, and central tissue necrosis. As there are intense efforts to develop clinical approaches to restore thymic medullary function in the adult to treat immunopathological conditions in which immune cell function is compromised following cancer therapy or toxin exposure, an improved molecular understanding of RANKL's involvement in thymic medulla enlargement will be required. We believe the versatility of the conditional *K5: RANKL* mouse represents a tractable model system to assist in addressing this requirement as well as many other questions related to RANKL's role in thymic normal physiology and disease processes.

Keywords

Thymus; Mouse; RANKL; Doxycycline; Cytokeratin 5; Cortex; Medulla; Transcriptome; RNA-seq

1. Introduction

Receptor Activator of NF-κB Ligand (RANKL) is a cytokine member of the tumor necrosis factor (TNF) superfamily [1–3]. The physiological and pathophysiological responses to RANKL (*Tnfsf 11*) are mediated through its cognate receptor RANK (*Tnfrsf 11a*), which, like RANKL, functions as a transmembrane homotrimer [4]. Apart from membrane bound RANKL, a cleaved RANKL ectodomain can also signal through its membrane receptor [5–8]. Following RANKL-RANK interaction, TNF-receptor associated factors (TRAFs) bind to the cytoplasmic portion of RANK to enable activation of distinct signaling cascades in a physiological-, tissue- and cell-context dependent fashion. Through paracrine and/or autocrine pathways, the RANKL/RANK signaling axis controls a broad spectrum of physiological processes, ranging from osteoclastogenesis and bone homeostasis, central whole-body thermoregulation to postnatal mammary gland morphogenesis, reviewed in [9]. Within the thymus, one of the earliest roles attributed to RANKL/RANK signaling was medullary thymic epithelial development, T-cell activation and dendritic cell survival, and promotion of immunotolerance [10–12].

To prevent autoimmunity, thymic central tolerance is developed by medullary thymic epithelial cells (mTECs) through a negative selection process that selects autoreactive thymocytes for clonal deletion by presenting a diverse array of tissue specific antigens (TSA) [13–15]. The negative selection process also promotes the generation of T regulatory cells (Tregs) and the intrathymic positioning of dendritic cells that are positive for the X-C motif chemokine ligand 1 (XCL1). The autoimmune regulator (AIRE), which is an mTEC transcriptional regulator, controls the ectopic expression of TSAs [16–19]. A number of studies have shown that RANKL, which is expressed in resident and recirculating mature T cells (single positive (SP) CD4+ cells and a small subset of CD8+ cells), as well as in invariant natural killer T (iNKT) cells and CD4+ CD3− lymphoid tissue inducer (LTi) cells, promotes expression of AIRE through the RANK receptor expressed in mTECs [20–22]. The induction of AIRE expression following RANKL/RANK engagement enables selection

of a diverse, functional and self-tolerant T cell repertoire that is essential for adaptive immunity [10–12, 23].

A number of conventional knockout and transgenic mouse models have been essential in demonstrating that the RANKL/RANK signaling axis is indispensable for the correct development and differentiation of mTECs, formation of the thymic medulla, and establishment of self-tolerance [20–22, 24–28]. Recent mouse-based investigations along with human studies have demonstrated that thymic RANKL/RANK signaling also controls placental immunotolerance and gestational diabetes to ensure normal establishment and maintenance of pregnancy [29]. Here, we report on the use of a recently generated bigenic mouse model (*K5: RANKL*) that can be used to conditionally express RANKL in cytokeratin 5 (K5) positive TECs when administered doxycycline (Dox). Induction of RANKL in K5 positive mTECs results in a striking increase in the size of both thymic lobes, which is due to a marked expansion of a hyperplastic thymic medulla accompanied by a decrease in cortical size. The medulla enlargement in the *K5: RANKL* thymus is associated with a significant increase in the number of CD4+ and CD8+ SP T cells, FOXP3+ Treg cells, and Ulex Europaeus Agglutinin-1 + (UEA1+) mTECs. However, the total number of thymocytes (including immature CD4+CD8+ double positive (DP) cells) is markedly reduced in the Dox-treated *K5: RANKL* thymus as a result of a significant size reduction in the thymocyte-enriched cortex. Transcriptomics revealed a striking alteration in the expression of a large number of genes, many of which are involved in immune processes and cellular proliferation, migration, invasion, tumorigenicity, and metastasis. With the unique ability to conditionally express RANKL in a spatiotemporal restricted manner, we believe that the versatile *K5: RANKL* bigenic mouse will serve as a useful addition to existing mouse models designed to study thymic RANKL signaling in normal and abnormal cellular contexts.

2. Materials and methods

2.1. The K5: RANKL bigenic

The generation of the *K5: RANKL* bigenic mouse was recently described [30]. Briefly, the K5-reverse tetracycline transactivator (*K5-rtTA*) effector transgenic mouse was crossed with our *TetO-RANKL* responder transgenic [31] to generate the *K5: RANKL* bigenic. In response to Dox-administration, the *K5: RANKL* mouse is designed to express transgene-derived RANKL in K5 positive epithelial cells. Both the *K5-rtTA* and *TetO-RANKL* transgenics are in the *FVB/NJ* inbred strain; the *K5-rtTA* transgenic spatially directs *rtTA* expression to K5 positive epithelial cells using a strong bovine keratin 5 (*KRT5*) promoter [32, 33]. Previous studies have successfully used the bovine K5 promoter to target transgene expression to K5+ mTECs of the mouse thymus [34]. For RANKL induction in the *K5: RANKL* bigenic, adult (8-9 week old) mice (along with monogenic effector and/or responder transgenics (herein referred to as controls)) were provided rodent chow containing Dox at 200 mg/kg (Bio-Serv, Flemington, NJ). Drinking water, containing 0.2% Dox (Takara BIO Inc., Mountain View, CA), was provided in light protected bottles [30]. To mitigate adverse taste effects, Dox supplemented water also included 5% sucrose. Freshly formulated Dox-supplemented water was provided every 3 days to avoid diminished

induction potency overtime. Depending on the experiment, Dox was administered for 48 hours or for 5-, 10-, or 42-days. Note: for some studies, controls also included *K5: RANKL* mice on regular food and water, referred to as: *K5: RANKL* (No Dox).

Mice were housed in an Association for Assessment and Accreditation of Laboratory Animal Care (AAALAC) accredited *vivarium* at Baylor College of Medicine. Within temperature-regulated animal housing units (22 ± 2 °C) with a 12-hour lights-on: 12-hour lights-off photocycle, mice received irradiated Tekland global soy protein-free extruded rodent diet (Harlan Laboratories, Inc., Indianapolis, IN) and fresh water *ad libitum*. Experiments on mice were conducted in accordance with the guidelines described in the Guide for the Care and Use of Laboratory Animals ("The Guide" (Eighth Edition 2011)), published by the National Research Council of the National Academies, Washington, D.C. The Institutional Animal Care and Use Committee (IACUC) at Baylor College of Medicine prospectively approved all mouse experiments.

2.2. Histological evaluation

Following overnight fixation in 4% paraformaldehyde, thymus tissue was paraffin-embedded using previously described procedures [30]. Sectioned to a 5μm thickness, paraffinized thymus tissue was placed on Superfrost Plus glass slides (ThermoFisher Scientific Inc., Waltham, MA). Prior to immunohistochemical staining, tissue sections were sequentially deparaffinized and rehydrated before treatment with an antigen unmasking solution. Following a blocking step, tissue sections were incubated with the requisite primary antibody overnight. Primary antibodies used in these experiments were: a rabbit polyclonal to human cytokeratin 5 (ab53121; (1:200), Abcam Inc., Cambridge, MA); a rabbit monoclonal to human cytokeratin 8 ((ab53280; (1:200) Abcam Inc.); a rabbit monoclonal anti-mouse AIRE antibody (EPR24411-22a (1:100); Abcam Inc.); a rabbit monoclonal anti-mouse FOXP3 antibody ((D608R) (1:200); Cell Signaling Technology Inc., Danvers, MA); sheep polyclonal to 5-bromo-2-deoxyuridine (BrdU) (ab1893 (1:100); Abcam Inc.); a goat polyclonal anti-mouse RANKL (TRANCE; AF462 (1: 200) R&D Systems, Minneapolis, MN). After primary antibody incubation, tissue sections were incubated with a compatible secondary antibody conjugated with horseradish peroxidase (Vector laboratories Inc., Burlingame, CA) for 1 h at room temperature. Immunopositivity was visually scored *in situ* through incubation with 3, 3'-diaminobenzidine (DAB, Vector laboratories Inc.); slides were lightly counterstained with hematoxylin for contrast. Following step-wise dehydration, slides were mounted with coverslips using Permount solution (ThermoFisher Scientific Inc., (SP15-500)). Using raw digital images captured at 200X and/or 400X magnification, Image J software (http://image.j.nih.gov/i.j./download.html) was used to count immunopositive cells per total 100 cells counted (immunopositive plus immunonegative). Three separate microscopic fields were counted per thymus tissue per mouse before the average percentage of positive cells was calculated. Unless otherwise specified, 3-4 mice per genotype were included in immunohistochemical studies described herein.

To immunohistochemically detect cellular incorporation of BrdU, mice received an intraperitoneal (I.P.) injection of BrdU (10 mg/ml; Amersham Biosciences Corporation, Piscataway, NJ) at a dose of 1mg BrdU/20g body weight two hours before euthanasia. For

dual immunofluorescence detection of K5 and RANKL protein expression, the following Alexa Fluor-conjugated secondary antibody combinations were used: Alexa Fluor Plus 584 donkey anti-rabbit IgG (A32754) and Alexa Fluor 488 donkey anti-goat IgG (A-11055) were used to detect K5 and RANKL respectively. Alexa Fluor-conjugated secondary antibodies were purchased from ThermoFisher Scientific Inc. Stained slides were mounted with coverslips using Vectashield mounting medium with 4', 6-diamidino-2-phenylindole (DAPI; (H-1200) Vector Laboratories Inc.). Raw digital images of immunostained thymus tissue sections were captured using a color chilled AxioCam MRc5 digital camera attached to a Carl Zeiss AxioImager A1 upright microscope (Zeiss, Jena, Germany). For data presentation, images were digitally collated and annotated using the latest version of Adobe Creative Suite software (Adobe Systems Inc., San Jose, CA).

2.3. Quantitative real-time PCR

Total RNA was extracted from thymus tissue using TRIzol reagent (ThermoFisher Scientific Inc.) with further purification using the RNeasy Plus Mini Kit (Qiagen Inc., Germantown Road, MD). Purified RNA was reversed transcribed into cDNA using the Superscript IV VILO Master Mix (ThermoFisher Scientific Inc.). The Applied Biosystems Step One Plus Real Time PCR system (ThermoFisher Scientific Inc.) was used for quantitative real-time PCR (qRT-PCR) amplification. Additional information on the TaqMan gene expression assays used in these experiments is provided in Table 1; ribosomal RNA 18S served as the internal control.

2.4. Thymic transcriptomic profiling

Similar to our previous RNA-sequencing (RNA-seq) experiments [30], NanoDrop spectrophotometry (ThermoFisher Scientific Inc.) assessed RNA purity while RNA integrity was evaluated using a 2100 Bioanalyzer with RNA chips (Agilent Technologies, Santa Clara, CA). Total RNA preparations with a RNA integrity number (RIN) of 8 or greater were used for RNA-seq. From 250ng of RNA, the TruSeq Stranded mRNA Library Prep kit (Ilumina, San Diego, CA) was used to prepare libraries for mRNA sequencing. Library quality was analyzed using the Agilent 4200 TapeStation with D1000 ScreenTape assays (Agilent Technologies). Using both a High Sensitivity DNA kit (Agilent Technologies) and the KAPA Library Quantification kit for Illumina platforms (KAPA Biosystems, Wilmington, MA), a 2100 Bioanalyzer quantitated pooled libraries. At the Gene and RNA Profiling (GARP) advance technology core at Baylor College of Medicine, sequencing of mRNA libraries was performed on an Illumina NextSeq 500 platform at mid-outpoint of paired-ended 75 base pair sequencing reads.

2.5. Bioinformatic analysis of sequenced thymic mRNA

Pair-ended reads were aligned to the mouse genome (UCSC mm10) using STAR open source software [35]; the NCBI RefSeq was used as the reference (gene expression was measured in read counts for each gene). The R package DESeq2 [36] was used to analyze the gene-based read counts to detect differently expressed genes between the monogenic control and *K5: RANKL* test groups on food and water supplemented with Dox. The false discovery rate (FDR) of differentially expressed genes was determined by the Benjamini and Hochberg method [37]; a FDR <0.05 was considered statistically significant. As detailed

in the Results section, due to the large number of differentially expressed genes with a FDR <0.05, a cut-off in the absolute fold change IFCI >5 and a sum of average counts >100 were used to further select genes for downstream analysis. Raw mRNA sequencing data were deposited in NCBI/GEO with the super series accession code: GSE123450. Gene ontology (GO) enrichment analysis for selected genes was performed using the Database for Annotation, Visualization and Integrated Discovery (DAVID) version 6.8 functional annotation clustering tool and the Kyoto Encyclopedia of Genes and Genomes (KEGG) pathway maps tool (http://david.ncifcrf.gov). For the enrichment analysis of Hallmark and Immune gene sets of the Molecular Signatures Database (https://www.gseamsigdb.org/gsea/index.jsp)), mouse entrez gene identification numbers were matched to human homologs using their HomoloGene IDs.

2.6. Flow cytometry and antibodies

Thymus tissue was dissected from *K5: RANKL* bigenics (with No Dox (control) or Dox (test) treatment) and immediately placed in PBS buffer on ice. Single-cell suspensions of thymocytes were prepared using previously described methods [38] . Thymocytes were blocked with CD16/32 (Fc receptor) before surface-stained in fluorescence-activated cell sorting (FACS) buffer (PBS, 2mM EDTA) for 30 min in the dark at 4°C. The following fluorophore-conjugated monoclonal antibodies were used: allophycocyanin (APC) rat anti-mouse CD4 (GK1.5 (100411)); fluorescein isothiocyanate (FITC) anti-mouse CD8a (53-6.7 (100705)); Brilliant Violet 711 (BV711-A) rat anti-mouse/human CD11b antibody (clone M1/70; 101241); Alexa Fluor 700 rat anti-mouse/human CD45R/B220 antibody (clone RA3-6B2; 103231) from Biolegend Inc., San Diego, CA. Brilliant violet 421 rat anti-mouse FOXP3 (clone MF-14; 126419), brilliant violet 605 rat anti-mouse CD4 (clone RM 4–5; 100547) and eFlour 450 rat anti-mouse FOXP3 (clone FJK-16s). Flow cytometry analyses were conducted using an LSRFortessa II cell analyzer (BD Biosciences Inc., Franklin Lakes, NJ) and data analyzed with FlowJo software (FlowJo LLC, Ashland, OR).

2.7. Western analysis

Western immunoblotting was conducted on protein isolates from thymus tissue by previously reported methods [30]. Thymic protein (20 μg) was separated by electrophoresis on a 4-15% gradient sodium dodecyl sulfate-polyacrylamide gel before electroblotting to polyvinylidene difluoride membranes (Bio-Rad Laboratories, Hercules, CA). The following primary antibodies (at a 1:1000 dilution) were used: goat polyclonal anti-mouse RANKL (AF462; R&D Systems) and a mouse monoclonal anti-human β-actin (Sigma-Aldrich, St. Louis, MO; A1978). Following the secondary antibody incubation and washes, immunopositive bands were detected using the SuperSignal West Pico Chemiluminescent Substrate kit (ThermoFisher Scientific Inc.).

2.8. Statistical analysis

When appropriate, the majority of the data is represented as the mean ± standard deviation (S.D.). Unless otherwise stated, the significance of the mean difference between two groups was calculated by the two-tailed Student's *t*-test (with a 95% confidence interval). A one-way ANOVA was used for analysis of three or more groups whereas a two-way ANOVA was used for analysis of three or more groups under different conditions. For a

subset of flow cytometry experiments, statistical analysis was performed using the Mann-Whitney nonparametric test. Statistical analysis was performed using the GraphPad and Instat statistical analysis tools (GraphPad Prism software Inc. La Jolla, CA). In most studies, at least three independent replicates were used (no samples were excluded). A probability (p)-value <0.05 was considered statistically significant; asterisks in histograms denote the level of significance: *p<0.05; **p<0.01; ***p<0.001; and ****p<0.0001

3. Results

3.1 Short-term doxycycline intake induces RANKL expression in the thymic medullary epithelium of the K5: RANKL bi-transgenic mouse

Compared to the monogenic control, both quantitative real-time PCR and western immunoblot analysis confirmed that transgene-derived RANKL expression is induced in the thymus of the *K5: RANKL* transgenic mouse following Dox-administration for forty-eight hours (Fig. 1A–C); this induction response agrees with our previous studies [30]. Results shown in Supplementary Fig. 1 further confirm that induction of transgene-derived RANKL in the *K5: RANKL* thymus is strictly dependent on Dox-administration. The latter result confirmed that *K5: RANKL* mice on regular chow and water can also serve as controls. Following this short-term Dox exposure period, immunohistochemical analysis revealed that the majority of Dox-induced RANKL expression occurs in the thymic medulla of the *K5: RANKL* bigenic (Fig. 1D–I). Dual immunofluorescence staining showed that transgene-derived RANKL expression is coincident with K5 expression in the thymic medulla of Dox-treated *K5: RANKL* bigenic mice (Fig. 1 J–M). Note that K5 positive mTECs adopt a stellate cellular organization pattern in the thymic medulla [34, 39–42]. Although forty-eight hours of Dox-administration induces a significant level of transgene-derived RANKL, aberrant changes at the histological and cellular level are not obvious in the *K5: RANKL* thymus compared with the control thymus.

3.2. Prolonged doxycycline administration results in significant thymic enlargement in the K5: RANKL mouse

In both male and female mice, ten days of Dox-administration significantly increased thymic tissue size in the *K5: RANKL* bigenic compared with control siblings (Fig. 2 A–B). Histological analysis of hematoxylin and eosin (H&E) stained tissue sections showed that the significantly increased size of the thymus in the Dox-treated *K5: RANKL* mouse is due to a marked enlargement of its medullary compartment (Fig. 2 (compare control (C) with *K5: RANKL* (D)). Immunohistochemical detection of BrdU positive cells showed a significant number of thymic medullary cells in the Dox-treated *K5: RANKL* mouse in S-phase of the cell cycle (Fig. 3A–G); however, with no significant difference in the number of proliferating cortical cells of the thymus from the control and *K5: RANKL* mouse (Fig. 3G). The latter result is interesting since transgene-derived RANKL is expressed in a small subset of K5 positive cTECs within the thymic cortex of the *K5: RANKL* transgenic (Supplementary Fig. 2). Following prolonged Dox-administration, transgene-derived RANKL expression becomes obvious due to a small population of K5 positive cells in the cortical thymic epithelial compartment (cTEC (Supplementary Fig. 3)) [13, 39, 41, 43]. However, because RANK is only expressed in mTECs [10, 21, 27, 29,

44–47], RANKL/RANK signaling in the thymic cortex fails to occur. Together, our results demonstrate a potent proliferative role for transgene-derived RANKL expressed in mTECs that drives thymic medulla expansion. The hyperproliferative medulla in the *K5: RANKL* thymus is also associated with a significant increase in the number of AIRE + mTECs and medullary FOXP3 + Tregs (Fig. 4). In normal thymus function, both cell types are strongly regulated by the cytokine actions of endogenous RANKL expressed from a number of T cell subclasses [21, 22, 27, 28, 48–52].

3.3. Immune cell population sizes are significantly altered in the K5: RANKL thymus

Flow cytometry shows that the percentage and absolute number of immune cell subtypes are significantly changed in the *K5: RANKL* thymus following 10 days of Dox-treatment (Dox) compared with *K5: RANKL* mice on a regular diet (No Dox) (Fig. 5). Total thymocyte number is significantly reduced in the Dox-treated *K5: RANKL* thymus (Fig. 5A), which reflects the marked reduction of cortical size along with significant medulla enlargement in response to transgene-derived RANKL induction. This result can be explained by the fact that the normal thymic cortex contains significantly more thymocytes compared with the medulla [14, 53, 54]. Therefore, a thymic cortical size reduction with a concomitant increase in medullary size will result in an overall depletion of thymocytes. However, there is a significant increase in the percentage of immune cells that are CD4+SP, CD8+SP and double negative (DN) in the *K5: RANKL* thymus following Dox-administration (Fig. 5B–D). This result can be explained by the observation that these immune cell types are normally located in the thymic medulla [13, 17, 19, 39, 47, 53, 55–57], which is the cellular compartment that is enlarged in the Dox-treated *K5: RANKL* thymus. One indication of thymic inflammation is a significant increase in the percentage and number of innate immune cells (*i.e.* B-cells, monocytes, and macrophages) in the Dox-treated *K5: RANKL* thymus (Fig. 5. E–H). Confirming our immunohistochemical results (Fig. 4), UEA1+ mTECs and FOXP3+ Tregs are significantly increased in the Dox-treated *K5: RANKL* thymus (Supplementary Fig. 4), again due to an enlarged thymic medulla. Whether these enriched immune cell types in the *K5: RANKL* thymus following Dox induction are phenotypically normal has yet be addressed. Notable, *K5: RANKL* mice lose significant body weight following persistent Dox-administration to 42 days (Supplementary Fig. 5). At this time period of Dox induction, histopathologic examination of the thymus revealed severe loss of normal organotypical features accompanied by extensive epithelial disorganization and hyperplasia within the medulla, central tissue necrosis and large macrophage infiltrates within dilated regions of the tissue; the cortical region is essentially absent (Supplementary Fig. 6). Despite this severe histopathology, the *K5: RANKL* thymus does not display indications of local invasion within the mediastinal region. Interestingly, our histomorphometric studies to date on peripheral lymphoid tissues (*i.e.* spleen) have not revealed overt abnormalities in the *K5: RANKL* bigenic (data not shown); however, a comprehensive analysis of all secondary/peripheral lymphoid tissues has yet to be completed.

3.4. Transcriptomics reveal the molecular underpinnings of the K5: RANKL thymic histopathologic phenotype

To identify the RANKL-responsive transcriptome that drives the *K5: RANKL* thymic histopathology, RNA-seq analyses was conducted on whole thymi from female monogenic

controls and female *K5: RANKL* bigenics, which were administered Dox-supplemented food and water for five days. Triplicates for both genotypes were used in the RNA-seq experiment in which all mice received Dox-supplemented food and water for 5 days (Fig. 6A). A 5-day Dox-treatment period was chosen as an approximate mid-point between short-term (48-hours (Fig. 1)) Dox-treatment when transgene-RANKL is clearly induced and 10-days of Dox-treatment when obvious histopathology is evident (Fig. 2). As an index of RNA-seq dataset quality, principal component analysis demonstrated that all samples tightly clustered according to their genotype (Fig. 6B). Using standard IFCI >2 and FDR <0.05 cutoffs, RNA-seq revealed that in excess of 10^5 genes were differentially expressed between the *K5: RANKL* and control groups (Supplementary File 1). Therefore, we applied a higher stringency of (IFCI >5; FDR< 0.05; and the sum of mean counts >100) to reduce the number of genes to 1723 in order to enable manageable downstream analysis (Supplementary File 1). Tables 2 and 3 list the top 50 genes for which expression is up or down regulated respectively between the two genotypes. Note: *RANKL* (*Tnfsf11*; entrez gene ID 21943), which is yellow highlighted in Table 2, is significantly upregulated (IFCI 127.671)) in the *K5: RANKL* thymus.

The above dataset was then compared to datasets from the Hallmark and Immune Collections of the Molecular Signatures Database (Fig. 7A and Supplementary File 1); human orthologs were identified through corresponding HomoloGene ID numbers. Gene Set Enrichment Analysis (GSEA) applied to the Hallmark collection showed that the expression of genes significantly changed in the *K5: RANKL* thymus when compared to the control thymus. Many of these genes are involved in a broad spectrum of biological and pathobiological processes that include epithelial-mesenchymal transition (EMT) that occurs in wound healing, fibrosis and metastasis; inflammation and immune responses, NF-κB signaling in response to tumor necrosis factor TNF signaling cues; KRAS signaling; and the innate immune system. Comparing this dataset with the Immunologic collection dataset revealed a significant enrichment of genes primarily expressed in the T cell repertoire. Reflecting the observed perturbation of the ultrastructure and signaling crosstalk in the *K5: RANKL* thymus, DAVID Functional Annotation Clustering (Fig. 7B) and Pathway analysis (Fig. 7C (left histogram)) highlighted a marked enrichment of genes associated with extracellular remodeling and tyrosine-protein kinase signaling. Importantly, KEGG pathway analysis (Fig. 7D) highlighted an increase in the percentage of genes involved in cytokine-cytokine receptor interaction, cell and focal adhesion, and components of the PI3K-AKT signaling pathway, which is a known effector pathway of RANKL/RANK signaling [58]. Using the Reactome database of reactions, pathways, and biological processes (https://reactome.org) [59] (Fig. 7C (right histogram)), integrin cell surface interactions and lymphoid-nonlymphoid cell interactions are prominently represented in the *K5: RANKL* thymus. The broad spectrum of biological, cellular, and molecular responses to RANKL induction predict that this myriad of signaling pathways and cellular processes collectively drive the *K5: RANKL* thymic phenotype.

3.5. Validation of potential molecular target expression in response to transgene-derived RANKL signaling in the K5: RANKL thymus

Our RNA-seq data revealed that a wide variety of genes, signaling pathways and biological processes potentially drive the thymic histopathology in the 5-day Dox-treated *K5: RANKL* bigenic. Quantitative real-time PCR analyses confirmed the increase in expression of a number of molecular targets in the *K5: RANKL* thymus that was predicted from our bioinformatic analyses above (Fig. 8). Male mice were used in the validation results shown (Fig. 8); female mice show the same result (data not shown). Displayed in alphabetical order are the results of an arbitrary chosen set of genes involved in immune, cytokine, NF-κB, and TNF signaling as well as molecular signals associated with aberrant tissue development and cancer. Apart from having documented roles in normal thymic immune development and function (see Discussion section below), many of these genes (when dysregulated) mediate pathological tissue responses. The list of genes in (Fig. 8) begin and end with AIRE and the RANKL/RANK cytokine signal respectively, both of which were previously shown to be altered in the *K5: RANKL* thymus (Fig. 4; Supplementary Figs. 2). In agreement with our previous immunohistochemical analyses (Figs. 4), AIRE is significantly induced in the Dox-treated *K5: RANKL* thymus when compared to the control (Fig. 8). Critical for immunotolerance [16, 18, 60–63], the AIRE zinc-finger transcription factor is known to be controlled by the RANKL/RANK signaling axis in mTECs [21]. Along with RANKL (*Tnfsf11*), its receptor RANK (*Tnfrsf11a*) is also significantly upregulated in the Dox-treated *K5: RANKL* thymus, reflecting the increase in the number of RANK+ mTECs in the *K5: RANKL* thymus [21]. Collectively, the results in (Fig. 8) validate the *K5: RANKL* thymic RNA-seq dataset as an important information resource for those investigators interested in thymic medullary crosstalk signaling in general, and in thymic RANKL/RANK signaling in particular.

4. Discussion

Similar to other thymic TNFSF cytokine ligands (*i.e.* TNFα; OX40L; CD40L; FASL; lymphotoxin (LT-α and LT-β); and CD30L [21]), RANKL expressed mainly from SP mature thymocytes binds its cognate receptor (RANK) within mTECs [21]. Previous mouse studies have shown that this RANKL/RANK signaling crosstalk between lymphocytes and medullary stroma is not only important for proliferation of mTECs in the postnatal thymus but also for the promotion of AIRE-mTECs progenitor cells into AIRE+ mTECs during embryogenesis [10]. While conventional knockout and transgenic mouse models have been instrumental in significantly advancing our understanding of RANKL/RANK signaling in normal and abnormal thymic function, the unique advantage of conditional transgenesis to this field has yet to be fully explored. This advantage includes the ability to express transgene-derived RANKL in a predetermined spatiotemporal manner during embryogenesis or in the postnatal mouse, during puberty or adulthood, and during changes in physiological states, such as pregnancy [64]. Also, the *K5: RANKL* transgenic crossed with the RANKL knockout mouse represents a feasible rescue approach by which the RANKL rescue signal can be spatiotemporally modulated. Moreover, *K5: RANKL* transgenic thymic cells could be used in an *in vitro* organoid system for the purposes of dissecting further the cellular

and molecular mechanisms of thymic RANKL action within a controlled cell-culture environment [65].

Here, we report findings from our initial thymic studies of the *K5: RANKL* conditional transgenic mouse. By conditionally targeting RANKL expression to the K5+ mTEC compartment in the adult mouse, we observed a significant enlargement of the thymic medulla following a 10 day Dox-treatment regimen. This finding inversely correlates with previous results that show a marked reduction of the thymic medulla following knockout of either RANKL or RANK, or following the use neutralizing antibodies to RANKL [20, 21]. Furthermore, the *K5: RANKL* thymic phenotype directly correlates with previous findings in the mouse that showed knockout of osteoprotegrin (OPG; a soluble decoy receptor for RANKL) or constitutively overexpression of soluble RANKL (sRANKL) result in a significant increase in the size of the murine mTEC compartment [11, 20, 21, 49, 66]. The size increase of the murine mTEC compartment following pharmacological administration of sRANKL also correlates with the *K5: RANKL* thymic phenotype reported here [67]. In the *K5: RANKL* bigenic, the observed mTEC proliferation resulting from transgene RANKL induction in K5+ mTECs most likely results from paracrine signaling from transgene RANKL (secreted or membrane-bound) to its endogenous cognate receptor, RANK, which is also expressed in mTECs [21]. Therefore, rather than normal RANKL/RANK crosstalk between mature thymocytes and the mTEC compartment [10, 21], the *K5: RANKL* thymic phenotype arises from RANKL/RANK signaling within the mTEC compartment. It's important to note that intra-epithelial paracrine crosstalk is a common feature of RANKL/RANK signaling in other target tissues, such as the mammary gland [31]. Since the AIRE-expressing mTEC compartment represents a microenvironment that normally provides an inductive milieu that is necessary for the final stages of T-cell differentiation [16–18, 21, 60, 61, 63, 68], it was not surprising to observe a striking enrichment of mature CD4+ and CD8+ SP cells in the *K5: RANKL* thymus arising from an expanded AIRE+ mTEC compartment. As an interesting corollary, because RANKL/RANK signaling enlarges the thymic medulla and increases CD4 and CD8 SP thymocyte cellularity, administration of RANKL has been considered as a possible pharmacological approach to boost thymic medulla regeneration and thymocyte reconstitution in patients in which lymphocytes in secondary or peripheral lymphoid tissues are destroyed by cancer therapeutics, toxins, or irradiation [67]. Therefore, an improved mechanistic understanding of RANKL-dependent thymic medulla expansion is required at the molecular level in order to uncover new avenues for the clinical modulation of self-tolerance and to guide the development of more effective therapeutic strategies to treat a number of immune disorders.

Thymic RNA-seq analysis of the 5-day Dox-treated *K5: RANKL* bigenic revealed an unusually large transcriptome, which is not surprising since the normal thymus transcriptionally expresses greater than 85% of its genome [10, 69]. The *K5: RANKL* thymic transcriptome is highly enriched for genes not only important for normal thymic homeostasis but also for abnormal tissue function and development, including cancer when dysregulated. Importantly, a significant subset of these genes is now being considered as possible therapeutic targets or as biomarkers for numerous disease processes. As selected examples from Figure 8, numerous cytokines, cytokine receptors, and chemokines are markedly enriched in the transcriptome of the Dox-treated *K5: RANKL* thymus.

In particular, the secreted C-C motif chemokine 8 (*Ccl8*, also known as monocyte chemoattractant protein 2 (*MCP-2*)) is a critical chemotactic factor for attracting monocytes [70]. Binding the *Ccr8*, *Ccl8* expression has been associated with invasion, tumorigenicity, stemness, and cancer metastasis [71–73]. Acting as a ligand for the C-C chemokine receptor (*Ccr6*), the C-C motif chemokine 20 (*Ccl20*) is responsible for the chemotaxis of dendritic cells, effector/memory T-cells and B-cells [74–77]. However, when deregulated, *Ccl20* also plays important roles in inflammation, cancer, and various autoimmune diseases [78–80]. Because it is expressed on multiple types of leukocytes, the CC chemokine receptor 1 (*CcR1*), which is a G-coupled receptor, has been considered as a target for autoimmune and inflammatory therapeutic applications [81]. An intercrine alpha (chemokine CXC) family member, the C-X-C motif chemokine 5 (*Cxcl5*) is involved in neutrophil activation following secretion from monocytes. Because of its implicated role in promoting the tumor microenvironment [82], the *Cxcl5/Cxcr2* axis has been examined not only as a biomarker but also as a potential therapeutic target for cancer therapy [83]. A chemotactic for interleukin-activated T-cells but not unstimulated T-cells, neutrophils or monocytes, the C-X-C motif chemokine 11 (*Cxcl11*) binds to *Cxcr3* to elicit T-cell recruitment. The *Cxcl11* has also been linked to promoting the tumor microenvironment [84].

Outside the cytokine/chemokine family, periostin (*Postn*, also known as osteoblast-specific factor 2) induces cell attachment and spreading with important roles in cell adhesion biology [85]. Acting as a multifunctional matricellular protein, *Postn* plays important roles in cancer development and progression [86, 87]. Parathyroid hormone-related protein (*PthrP*, also known as osteostatin) is a neuroendocrine peptide which is an essential regulator of intercellular signaling for organ growth, such as epithelial-mesenchymal interactions during the embryonic formation of the mammary gland [88]. Interestingly, *PthrP* has been shown to cooperate with soluble RANKL signaling in other physiological systems, such as regulating the osteogenesis of bone mesenchymal stem cells [89]. Moreover, we recently showed that *Postn* and *PthrP* as well as *SPP1* (below) are induced in the *K5: RANKL* salivary gland [30]. A member of the *Rel/NF-κB* family of transcription factors [90], the *Relb* transcription factor is associated with a plethora of biological responses that include antigen processing and presentation, inflammatory responses, innate immune responses, lymphocyte differentiation, myeloid dendritic cell differentiation, negative regulation of interferon-beta production, cytokine responses, and T-helper cell differentiation [90–92]. Not surprisingly, Relb dysregulation has been associated with cancer [93]. Interesting, *Relb* function is essential for the emergence of RANK+ medullary epithelial progenitor cell type [94]. Receptor expressed in lymphoid tissue (*Relt*) is also a member of the tumor necrosis factor receptor superfamily (TNFRSF) [95] and known to activate NFκB signaling to promote growth of carcinomas [96]. The binding partner of *Relt* (*Relt-like 1* (*Rell1*)) is now considered an oncogene in accelerating the growth of certain cancers [97]. Similar to *Postn* above, secreted phosphoprotein 1 (*Spp1*; also known as osteopontin*)* is critical for cell-matrix interactions and has been linked to various stages of cancer progression [87, 98, 99]. Lastly, tumor necrosis factor alpha-induced protein 2 (*Tnfaip2*) is a primary response gene to TNFα, expressed in multiple immune cells, and regulated by multiple transcription factors, including NF-kB [100]. Because of its roles in cell proliferation, migration, invasion,

and angiogenesis, Tnfaip2 has been associated with a number of cancers and infectious diseases [101].

With prolonged Dox induction, the *K5: RANKL* thymic medulla significantly enlarges to an extent that the peripheral cortex is markedly diminished. Although significant medullary epithelial hyperplasia is evident along with a massive infiltration of inflammatory immune cells, the tissue does not display obvious histological features of thymic epithelial tumors following this time period of Dox treatment [102]. Being the most frequent masses of the anterior mediastinum, thymomas and thymic carcinomas are rare thymic epithelial tumors that display different histological subtypes and clinical behaviors [102]. It's possible that a longer time period of Dox treatment is required (> 6-weeks) to observe the emergence of thymic epithelial tumors. However, because these mice experience significant weight loss by 6-weeks of Dox administration, transplantation of the *K5: RANKL* thymus into Dox-treated isogenic host mice would be necessary to extend the time of Dox induction [103–108].

In summary, the *K5: RANKL* bigenic described here is a new addition to mouse models that have been engineered to investigate RANKL/RANK signaling in thymus biology and pathobiology. The *K5: RANKL* transgenic provides distinct advantages of conditional transgenesis that enables spatiotemporal control of thymic RANKL expression. Through use of short-, medium-, and long-term RANKL induction periods, markedly different thymic phenotypes can be generated. The transcriptome that drives the *K5: RANKL* thymic phenotype following 5-days of Dox administration is predicted to be a rich source of molecular information that will enhance our future mechanistic understanding of thymic RANKL/RANK signaling. Moreover, this transcriptome constitutes an invaluable reference for future *K5: RANKL* thymic transcript profiling experiments that are conducted following shorter time periods of Dox administration as well as serving as a foundational information resource for future single-cell and spatial transcriptomic approaches.

Supplementary Material

Refer to Web version on PubMed Central for supplementary material.

Acknowledgements

We are grateful for the invaluable technical assistance provided by Yan Ying and Rong Zhao. The flow cytometry experiments were conducted in part by the Cytometry and Cell Sorting Core at Baylor College of Medicine with funding from the National Institutes of Health (NIH: A1036211; CA12523; and RR024574). The RNA-seq studies were performed by the Genomic and RNA Profiling Core at Baylor College of Medicine with funding from the NIH NCI (P30CA125123) and CPRIT (RP200504) grants. The histopathology analyses were conducted by the Integrated Biospecimen Shared Resource, supported by the NIH/NCI to the Dan L. Duncan Cancer Center (P30 CA125123). Finally, this research was funded in part by the NIH/National Institute of Diabetes & Digestive and Kidney Diseases (NIH/NIDDK grant: R01 DK119352-01 to MLB) and by the NIH/National Institute of Child Health and Human Development (NIH/NICHD grant: R01 HD042311 to JPL).

References

1. Dougall WC, Chaisson M. The RANK/RANKL/OPG triad in cancer-induced bone diseases. Cancer Metastasis Rev. 2006;25(4):541–9. [PubMed: 17180711]
2. Fernandez-Valdivia R, Lydon JP. From the ranks of mammary progesterone mediators, RANKL takes the spotlight. Mol Cell Endocrinol. 2012;357(1-2):91–100. [PubMed: 21964466]

3. Walsh MC, Choi Y. Biology of the RANKL-RANK-OPG System in Immunity, Bone, and Beyond. Front Immunol. 2014;5:511. [PubMed: 25368616]
4. Douni E, Rinotas V, Makrinou E, Zwerina J, Penninger JM, Eliopoulos E, et al. A RANKL G278R mutation causing osteopetrosis identifies a functional amino acid essential for trimer assembly in RANKL and TNF. Hum Mol Genet. 2012;21(4):784–98. [PubMed: 22068587]
5. Greenhill C. Function of soluble RANKL deciphered. Nat Rev Endocrinol. 2019;15(11):628.
6. Asano T, Okamoto K, Nakai Y, Tsutsumi M, Muro R, Suematsu A, et al. Soluble RANKL is physiologically dispensable but accelerates tumour metastasis to bone. Nat Metab. 2019;1(9):868–75. [PubMed: 32694743]
7. Elango J, Bao B, Wu W. The hidden secrets of soluble RANKL in bone biology. Cytokine. 2021;144:155559. [PubMed: 33994070]
8. Nakashima T, Kobayashi Y, Yamasaki S, Kawakami A, Eguchi K, Sasaki H, et al. Protein expression and functional difference of membrane-bound and soluble receptor activator of NF-kappaB ligand: modulation of the expression by osteotropic factors and cytokines. Biochem Biophys Res Commun. 2000;275(3):768–75. [PubMed: 10973797]
9. Rao S, Cronin SJF, Sigl V, Penninger JM. RANKL and RANK: From Mammalian Physiology to Cancer Treatment. Trends Cell Biol. 2018;28(3):213–23. [PubMed: 29241686]
10. Irla M. RANK Signaling in the Differentiation and Regeneration of Thymic Epithelial Cells. Front Immunol. 2020;11:623265. [PubMed: 33552088]
11. Ohigashi I, Nitta T, Lkhagvasuren E, Yasuda H, Takahama Y. Effects of RANKL on the thymic medulla. Eur J Immunol. 2011;41(7):1822–7. [PubMed: 21706487]
12. Walsh MC, Choi Y. Regulation of T cell-associated tissues and T cell activation by RANKL-RANK-OPG. J Bone Miner Metab. 2021;39(1):54–63. [PubMed: 33438173]
13. Anderson G, Takahama Y. Thymic epithelial cells: working class heroes for T cell development and repertoire selection. Trends Immunol. 2012;33(6):256–63. [PubMed: 22591984]
14. Koch U, Radtke F. Mechanisms of T cell development and transformation. Annu Rev Cell Dev Biol. 2011;27:539–62. [PubMed: 21740230]
15. Sun L, Luo H, Li H, Zhao Y. Thymic epithelial cell development and differentiation: cellular and molecular regulation. Protein Cell. 2013;4(5):342–55. [PubMed: 23589020]
16. Anderson MS, Venanzi ES, Klein L, Chen Z, Berzins SP, Turley SJ, et al. Projection of an immunological self shadow within the thymus by the aire protein. Science. 2002;298(5597):1395–401. [PubMed: 12376594]
17. Irla M, Hugues S, Gill J, Nitta T, Hikosaka Y, Williams IR, et al. Autoantigen-specific interactions with CD4+ thymocytes control mature medullary thymic epithelial cell cellularity. Immunity. 2008;29(3):451–63. [PubMed: 18799151]
18. Perniola R. Twenty Years of AIRE. Front Immunol. 2018;9:98. [PubMed: 29483906]
19. Shevyrev D, Tereshchenko V, Kozlov V, Sennikov S. Phylogeny, Structure, Functions, and Role of AIRE in the Formation of T-Cell Subsets. Cells. 2022;11(2).
20. Akiyama T, Shimo Y, Yanai H, Qin J, Ohshima D, Maruyama Y, et al. The tumor necrosis factor family receptors RANK and CD40 cooperatively establish the thymic medullary microenvironment and self-tolerance. Immunity. 2008;29(3):423–37. [PubMed: 18799149]
21. Hikosaka Y, Nitta T, Ohigashi I, Yano K, Ishimaru N, Hayashi Y, et al. The cytokine RANKL produced by positively selected thymocytes fosters medullary thymic epithelial cells that express autoimmune regulator. Immunity. 2008;29(3):438–50. [PubMed: 18799150]
22. Roberts NA, White AJ, Jenkinson WE, Turchinovich G, Nakamura K, Withers DR, et al. Rank signaling links the development of invariant gammadelta T cell progenitors and Aire(+) medullary epithelium. Immunity. 2012;36(3):427–37. [PubMed: 22425250]
23. Sobacchi C, Menale C, Villa A. The RANKL-RANK Axis: A Bone to Thymus Round Trip. Front Immunol. 2019;10:629. [PubMed: 30984193]
24. Dougall WC, Glaccum M, Charrier K, Rohrbach K, Brasel K, De Smedt T, et al. RANK is essential for osteoclast and lymph node development. Genes Dev. 1999;13(18):2412–24. [PubMed: 10500098]

25. Kim N, Odgren PR, Kim DK, Marks SC Jr., Choi Y. Diverse roles of the tumor necrosis factor family member TRANCE in skeletal physiology revealed by TRANCE deficiency and partial rescue by a lymphocyte-expressed TRANCE transgene. Proc Natl Acad Sci U S A. 2000;97(20):10905–10. [PubMed: 10984520]
26. Kong YY, Yoshida H, Sarosi I, Tan HL, Timms E, Capparelli C, et al. OPGL is a key regulator of osteoclastogenesis, lymphocyte development and lymph-node organogenesis. Nature. 1999;397(6717):315–23. [PubMed: 9950424]
27. McCarthy NI, Cowan JE, Nakamura K, Bacon A, Baik S, White AJ, et al. Osteoprotegerin-Mediated Homeostasis of Rank+ Thymic Epithelial Cells Does Not Limit Foxp3+ Regulatory T Cell Development. J Immunol. 2015;195(6):2675–82. [PubMed: 26254339]
28. Rossi SW, Kim MY, Leibbrandt A, Parnell SM, Jenkinson WE, Glanville SH, et al. RANK signals from CD4(+)3(−) inducer cells regulate development of Aire-expressing epithelial cells in the thymic medulla. J Exp Med. 2007;204(6):1267–72. [PubMed: 17502664]
29. Paolino M, Koglgruber R, Cronin SJF, Uribesalgo I, Rauscher E, Harreiter J, et al. RANK links thymic regulatory T cells to fetal loss and gestational diabetes in pregnancy. Nature. 2021;589(7842):442–7. [PubMed: 33361811]
30. Hai L, Szwarc MM, Lonard DM, Rajapakshe K, Perera D, Coarfa C, et al. Short-term RANKL exposure initiates a neoplastic transcriptional program in the basal epithelium of the murine salivary gland. Cytokine. 2019;123:154745. [PubMed: 31226438]
31. Mukherjee A, Soyal SM, Li J, Ying Y, He B, DeMayo FJ, et al. Targeting RANKL to a specific subset of murine mammary epithelial cells induces ordered branching morphogenesis and alveologenesis in the absence of progesterone receptor expression. FASEB J. 2010;24(11):4408–19. [PubMed: 20605949]
32. Raimondi AR, Vitale-Cross L, Amornphimoltham P, Gutkind JS, Molinolo A. Rapid development of salivary gland carcinomas upon conditional expression of K-ras driven by the cytokeratin 5 promoter. Am J Pathol. 2006;168(5):1654–65. [PubMed: 16651631]
33. Vitale-Cross L, Amornphimoltham P, Fisher G, Molinolo AA, Gutkind JS. Conditional expression of K-ras in an epithelial compartment that includes the stem cells is sufficient to promote squamous cell carcinogenesis. Cancer Res. 2004;64(24):8804–7. [PubMed: 15604235]
34. Lomada D, Liu B, Coghlan L, Hu Y, Richie ER. Thymus medulla formation and central tolerance are restored in IKKalpha−/− mice that express an IKKalpha transgene in keratin 5+ thymic epithelial cells. J Immunol. 2007;178(2):829–37. [PubMed: 17202344]
35. Dobin A, Davis CA, Schlesinger F, Drenkow J, Zaleski C, Jha S, et al. STAR: ultrafast universal RNA-seq aligner. Bioinformatics. 2013;29(1):15–21. [PubMed: 23104886]
36. Love MI, Huber W, Anders S. Moderated estimation of fold change and dispersion for RNA-seq data with DESeq2. Genome Biol. 2014;15(12):550. [PubMed: 25516281]
37. Benjamini Y Controlling the false discovery rate: a practical and poweful approach to multiple testing. In: Hochberg Y, editor.: J. Royal Statistical Society; 1995. p. 289–300.
38. Xing Y, Hogquist KA. Isolation, identification, and purification of murine thymic epithelial cells. J Vis Exp. 2014(90):e51780. [PubMed: 25145384]
39. Danzl NM, Jeong S, Choi Y, Alexandropoulos K. Identification of novel thymic epithelial cell subsets whose differentiation is regulated by RANKL and Traf6. PLoS One. 2014;9(1):e86129. [PubMed: 24465914]
40. Klug DB, Carter C, Crouch E, Roop D, Conti CJ, Richie ER. Interdependence of cortical thymic epithelial cell differentiation and T-lineage commitment. Proc Natl Acad Sci U S A. 1998;95(20):11822–7. [PubMed: 9751749]
41. Popa I, Zubkova I, Medvedovic M, Romantseva T, Mostowski H, Boyd R, et al. Regeneration of the adult thymus is preceded by the expansion of K5+K8+ epithelial cell progenitors and by increased expression of Trp63, cMyc and Tcf3 transcription factors in the thymic stroma. Int Immunol. 2007;19(11):1249–60. [PubMed: 17823311]
42. Sawanobori Y, Ueta H, Dijkstra CD, Park CG, Satou M, Kitazawa Y, et al. Three distinct subsets of thymic epithelial cells in rats and mice defined by novel antibodies. PLoS One. 2014;9(10):e109995. [PubMed: 25334032]

43. Odaka C, Loranger A, Takizawa K, Ouellet M, Tremblay MJ, Murata S, et al. Keratin 8 is required for the maintenance of architectural structure in thymus epithelium. PLoS One. 2013;8(9):e75101. [PubMed: 24086449]
44. Desanti GE, Cowan JE, Baik S, Parnell SM, White AJ, Penninger JM, et al. Developmentally regulated availability of RANKL and CD40 ligand reveals distinct mechanisms of fetal and adult cross-talk in the thymus medulla. J Immunol. 2012;189(12):5519–26. [PubMed: 23152561]
45. Lee HW, Park HK, Na YJ, Kim CD, Lee JH, Kim BS, et al. RANKL stimulates proliferation, adhesion and IL-7 expression of thymic epithelial cells. Exp Mol Med. 2008;40(1):59–70. [PubMed: 18305399]
46. Montero-Herradon S, Garcia-Ceca J, Zapata AG. Altered Maturation of Medullary TEC in EphB-Deficient Thymi Is Recovered by RANK Signaling Stimulation. Front Immunol. 2018;9:1020. [PubMed: 29867988]
47. Nitta T, Ohigashi I, Nakagawa Y, Takahama Y. Cytokine crosstalk for thymic medulla formation. Curr Opin Immunol. 2011;23(2):190–7. [PubMed: 21194915]
48. Bichele R, Kisand K, Peterson P, Laan M. TNF superfamily members play distinct roles in shaping the thymic stromal microenvironment. Mol Immunol. 2016;72:92–102. [PubMed: 27011037]
49. Khan IS, Mouchess ML, Zhu ML, Conley B, Fasano KJ, Hou Y, et al. Enhancement of an anti-tumor immune response by transient blockade of central T cell tolerance. J Exp Med. 2014;211(5):761–8. [PubMed: 24752296]
50. Su MA, Anderson MS. Pulling RANK on Cancer: Blocking Aire-Mediated Central Tolerance to Enhance Immunotherapy. Cancer Immunol Res. 2019;7(6):854–9. [PubMed: 31160305]
51. White AJ, Withers DR, Parnell SM, Scott HS, Finke D, Lane PJ, et al. Sequential phases in the development of Aire-expressing medullary thymic epithelial cells involve distinct cellular input. Eur J Immunol. 2008;38(4):942–7. [PubMed: 18350550]
52. Lin J, Yang L, Silva HM, Trzeciak A, Choi Y, Schwab SR, et al. Increased generation of Foxp3(+) regulatory T cells by manipulating antigen presentation in the thymus. Nat Commun. 2016;7:10562. [PubMed: 26923114]
53. Nitta T, Murata S, Ueno T, Tanaka K, Takahama Y. Thymic microenvironments for T-cell repertoire formation. Adv Immunol. 2008;99:59–94. [PubMed: 19117532]
54. Zdrojewicz Z, Pachura E, Pachura P. The Thymus: A Forgotten, But Very Important Organ. Adv Clin Exp Med. 2016;25(2):369–75. [PubMed: 27627572]
55. Irla M, Guerri L, Guenot J, Serge A, Lantz O, Liston A, et al. Antigen recognition by autoreactive CD4(+) thymocytes drives homeostasis of the thymic medulla. PLoS One. 2012;7(12):e52591. [PubMed: 23300712]
56. Kong YY, Boyle WJ, Penninger JM. Osteoprotegerin ligand: a common link between osteoclastogenesis, lymph node formation and lymphocyte development. Immunol Cell Biol. 1999;77(2):188–93. [PubMed: 10234557]
57. Naquet P, Naspetti M, Boyd R. Development, organization and function of the thymic medulla in normal, immunodeficient or autoimmune mice. Semin Immunol. 1999;11(1):47–55. [PubMed: 9950751]
58. Wong BR, Besser D, Kim N, Arron JR, Vologodskaia M, Hanafusa H, et al. TRANCE, a TNF family member, activates Akt/PKB through a signaling complex involving TRAF6 and c-Src. Mol Cell. 1999;4(6):1041–9. [PubMed: 10635328]
59. Fabregat A, Jupe S, Matthews L, Sidiropoulos K, Gillespie M, Garapati P, et al. The Reactome Pathway Knowledgebase. Nucleic Acids Res. 2018;46(D1):D649–D55. [PubMed: 29145629]
60. Anderson MS, Su MA. AIRE expands: new roles in immune tolerance and beyond. Nat Rev Immunol. 2016;16(4):247–58. [PubMed: 26972725]
61. Chan AY, Anderson MS. Central tolerance to self revealed by the autoimmune regulator. Ann N Y Acad Sci. 2015;1356:80–9. [PubMed: 26579596]
62. Proekt I, Miller CN, Lionakis MS, Anderson MS. Insights into immune tolerance from AIRE deficiency. Curr Opin Immunol. 2017;49:71–8. [PubMed: 29065385]
63. Yano M, Kuroda N, Han H, Meguro-Horike M, Nishikawa Y, Kiyonari H, et al. Aire controls the differentiation program of thymic epithelial cells in the medulla for the establishment of self-tolerance. J Exp Med. 2008;205(12):2827–38. [PubMed: 19015306]

64. Lewandoski M. Conditional control of gene expression in the mouse. Nat Rev Genet. 2001;2(10):743–55. [PubMed: 11584291]
65. Tajima A, Pradhan I, Geng X, Trucco M, Fan Y. Construction of Thymus Organoids from Decellularized Thymus Scaffolds. Methods Mol Biol. 2019;1576:33–42. [PubMed: 27730537]
66. Tsukasaki M, Asano T, Muro R, Huynh NC, Komatsu N, Okamoto K, et al. OPG Production Matters Where It Happened. Cell Rep. 2020;32(10):108124. [PubMed: 32905763]
67. Lopes N, Vachon H, Marie J, Irla M. Administration of RANKL boosts thymic regeneration upon bone marrow transplantation. EMBO Mol Med. 2017;9(6):835–51. [PubMed: 28455312]
68. Meredith M, Zemmour D, Mathis D, Benoist C. Aire controls gene expression in the thymic epithelium with ordered stochasticity. Nat Immunol. 2015;16(9):942–9. [PubMed: 26237550]
69. Sansom SN, Shikama-Dorn N, Zhanybekova S, Nusspaumer G, Macaulay IC, Deadman ME, et al. Population and single-cell genomics reveal the Aire dependency, relief from Polycomb silencing, and distribution of self-antigen expression in thymic epithelia. Genome Res. 2014;24(12):1918–31. [PubMed: 25224068]
70. Farmaki E, Chatzistamou I, Kaza V, Kiaris H. A CCL8 gradient drives breast cancer cell dissemination. Oncogene. 2016;35(49):6309–18. [PubMed: 27181207]
71. Barbai T, Fejos Z, Puskas LG, Timar J, Raso E. The importance of microenvironment: the role of CCL8 in metastasis formation of melanoma. Oncotarget. 2015;6(30):29111–28. [PubMed: 26320180]
72. Chen XJ, Deng YR, Wang ZC, Wei WF, Zhou CF, Zhang YM, et al. Hypoxia-induced ZEB1 promotes cervical cancer progression via CCL8-dependent tumour-associated macrophage recruitment. Cell Death Dis. 2019;10(7):508. [PubMed: 31263103]
73. Zhang X, Chen L, Dang WQ, Cao MF, Xiao JF, Lv SQ, et al. CCL8 secreted by tumor-associated macrophages promotes invasion and stemness of glioblastoma cells via ERK1/2 signaling. Lab Invest. 2020;100(4):619–29. [PubMed: 31748682]
74. Rohrl J, Yang D, Oppenheim JJ, Hehlgans T. Specific binding and chemotactic activity of mBD4 and its functional orthologue hBD2 to CCR6-expressing cells. J Biol Chem. 2010;285(10):7028–34. [PubMed: 20068036]
75. Schutyser E, Struyf S, Menten P, Lenaerts JP, Conings R, Put W, et al. Regulated production and molecular diversity of human liver and activation-regulated chemokine/macrophage inflammatory protein-3 alpha from normal and transformed cells. J Immunol. 2000;165(8):4470–7. [PubMed: 11035086]
76. Nelson RT, Boyd J, Gladue RP, Paradis T, Thomas R, Cunningham AC, et al. Genomic organization of the CC chemokine mip-3alpha/CCL20/larc/exodus/SCYA20, showing gene structure, splice variants, and chromosome localization. Genomics. 2001;73(1):28–37. [PubMed: 11352563]
77. Lee AYS, Korner H. The CCR6-CCL20 axis in humoral immunity and T-B cell immunobiology. Immunobiology. 2019;224(3):449–54. [PubMed: 30772094]
78. Ito T, Carson WFt, Cavassani KA, Connett JM, Kunkel SL. CCR6 as a mediator of immunity in the lung and gut. Exp Cell Res. 2011;317(5):613–9. [PubMed: 21376174]
79. Kadomoto S, Izumi K, Mizokami A. The CCL20-CCR6 Axis in Cancer Progression. Int J Mol Sci. 2020;21(15).
80. Kwantwi LB, Wang S, Sheng Y, Wu Q. Multifaceted roles of CCL20 (C-C motif chemokine ligand 20): mechanisms and communication networks in breast cancer progression. Bioengineered. 2021;12(1):6923–34. [PubMed: 34569432]
81. Gilchrist A, Echeverria SL. Targeting Chemokine Receptor CCR1 as a Potential Therapeutic Approach for Multiple Myeloma. Front Endocrinol (Lausanne). 2022;13:846310. [PubMed: 35399952]
82. Swamydas M, Ricci K, Rego SL, Dreau D. Mesenchymal stem cell-derived CCL-9 and CCL-5 promote mammary tumor cell invasion and the activation of matrix metalloproteinases. Cell Adh Migr. 2013;7(3):315–24. [PubMed: 23722213]
83. Zhang W, Wang H, Sun M, Deng X, Wu X, Ma Y, et al. CXCL5/CXCR2 axis in tumor microenvironment as potential diagnostic biomarker and therapeutic target. Cancer Commun (Lond). 2020;40(2-3):69–80. [PubMed: 32237072]

84. Gao Q, Zhang Y. CXCL11 Signaling in the Tumor Microenvironment. Adv Exp Med Biol. 2021;1302:41–50. [PubMed: 34286440]
85. Conway SJ, Izuhara K, Kudo Y, Litvin J, Markwald R, Ouyang G, et al. The role of periostin in tissue remodeling across health and disease. Cell Mol Life Sci. 2014;71(7):1279–88. [PubMed: 24146092]
86. Yu Y, Tan CM, Jia YY. Research status and the prospect of POSTN in various tumors. Neoplasma. 2021;68(4):673–82. [PubMed: 34348466]
87. Gonzalez-Gonzalez L, Alonso J. Periostin: A Matricellular Protein With Multiple Functions in Cancer Development and Progression. Front Oncol. 2018;8:225. [PubMed: 29946533]
88. Hiremath M, Wysolmerski J. Parathyroid hormone-related protein specifies the mammary mesenchyme and regulates embryonic mammary development. J Mammary Gland Biol Neoplasia. 2013;18(2):171–7. [PubMed: 23640717]
89. Elango J, Rahman SU, Henrotin Y, de Val J, Bao B, Wang S, et al. Parathyroid Hormone-Related Protein (PTHrP) Accelerates Soluble RANKL Signals for Downregulation of Osteogenesis of Bone Mesenchymal Stem Cells. J Clin Med. 2019;8(6).
90. Ryseck RP, Weih F, Carrasco D, RelB Bravo R., a member of the Rel/NF-kappa B family of transcription factors. Braz J Med Biol Res. 1996;29(7):895–903. [PubMed: 9070378]
91. Ghosh S, May MJ, Kopp EB. NF-kappa B and Rel proteins: evolutionarily conserved mediators of immune responses. Annu Rev Immunol. 1998;16:225–60. [PubMed: 9597130]
92. Zanetti M, Castiglioni P, Schoenberger S, Gerloni M. The role of relB in regulating the adaptive immune response. Ann N Y Acad Sci. 2003;987:249–57. [PubMed: 12727647]
93. Rayet B, Gelinas C. Aberrant rel/nfkb genes and activity in human cancer. Oncogene. 1999;18(49):6938–47. [PubMed: 10602468]
94. Baik S, Sekai M, Hamazaki Y, Jenkinson WE, Anderson G. Relb acts downstream of medullary thymic epithelial stem cells and is essential for the emergence of RANK(+) medullary epithelial progenitors. Eur J Immunol. 2016;46(4):857–62. [PubMed: 26806881]
95. Sica GL, Zhu G, Tamada K, Liu D, Ni J, Chen L. RELT, a new member of the tumor necrosis factor receptor superfamily, is selectively expressed in hematopoietic tissues and activates transcription factor NF-kappaB. Blood. 2001;97(9):2702–7. [PubMed: 11313261]
96. Yao W, Chen Q, Li S, Jia X, Xu L, Wei L. RELT promotes the growth of esophageal squamous cell carcinoma by activating the NF-kappaB pathway. Cell Cycle. 2021;20(13):1231–41. [PubMed: 34121605]
97. Jin X, Xie H, Liu X, Shen Q, Wang Z, Hao H, et al. RELL1, a novel oncogene, accelerates tumor progression and regulates immune infiltrates in glioma. Int Immunopharmacol. 2020;87:106707. [PubMed: 32683297]
98. Lamort AS, Giopanou I, Psallidas I, Stathopoulos GT. Osteopontin as a Link between Inflammation and Cancer: The Thorax in the Spotlight. Cells. 2019;8(8).
99. Pang X, Gong K, Zhang X, Wu S, Cui Y, Qian BZ. Osteopontin as a multifaceted driver of bone metastasis and drug resistance. Pharmacol Res. 2019;144:235–44. [PubMed: 31028902]
100. Guo F, Yuan Y. Tumor Necrosis Factor Alpha-Induced Proteins in Malignant Tumors: Progress and Prospects. Onco Targets Ther. 2020;13:3303–18. [PubMed: 32368089]
101. Jia L, Shi Y, Wen Y, Li W, Feng J, Chen C. The roles of TNFAIP2 in cancers and infectious diseases. J Cell Mol Med. 2018;22(11):5188–95. [PubMed: 30145807]
102. Marx A, Chan JKC, Chalabreysse L, Dacic S, Detterbeck F, French CA, et al. The 2021 WHO Classification of Tumors of the Thymus and Mediastinum: What Is New in Thymic Epithelial, Germ Cell, and Mesenchymal Tumors? J Thorac Oncol. 2022;17(2):200–13. [PubMed: 34695605]
103. Hong R Thymus transplantation. Birth Defects Orig Artic Ser. 1983;19(3):259–65. [PubMed: 6360237]
104. Jones GV, Botham CA, Kendall MD. Use of cultured thymic tissues for the regeneration of the thymus. Neuroimmunomodulation. 1999;6(1-2):6–22. [PubMed: 9876230]
105. Ikehara S Thymus transplantation for treatment of cancer: lessons from murine models. Expert Rev Clin Immunol. 2011;7(2):205–11. [PubMed: 21426258]

106. Hosaka N New allogeneic hematopoietic stem cell transplantation method: hematopoietic stem cell transplantation plus thymus transplantation for intractable diseases. Clin Dev Immunol. 2013;2013:545621. [PubMed: 23762092]

107. Peaudecerf L, Krenn G, Goncalves P, Vasseur F, Rocha B. Thymocytes self-renewal: a major hope or a major threat? Immunol Rev. 2016;271(1):173–84. [PubMed: 27088914]

108. Hosaka N Role of Regulatory T Cells in Tumor-Bearing Mice Treated with Allo-Hematopoietic Stem Cell Transplantation Plus Thymus Transplantation. J Immunol Res. 2018;2018:7271097. [PubMed: 30057919]

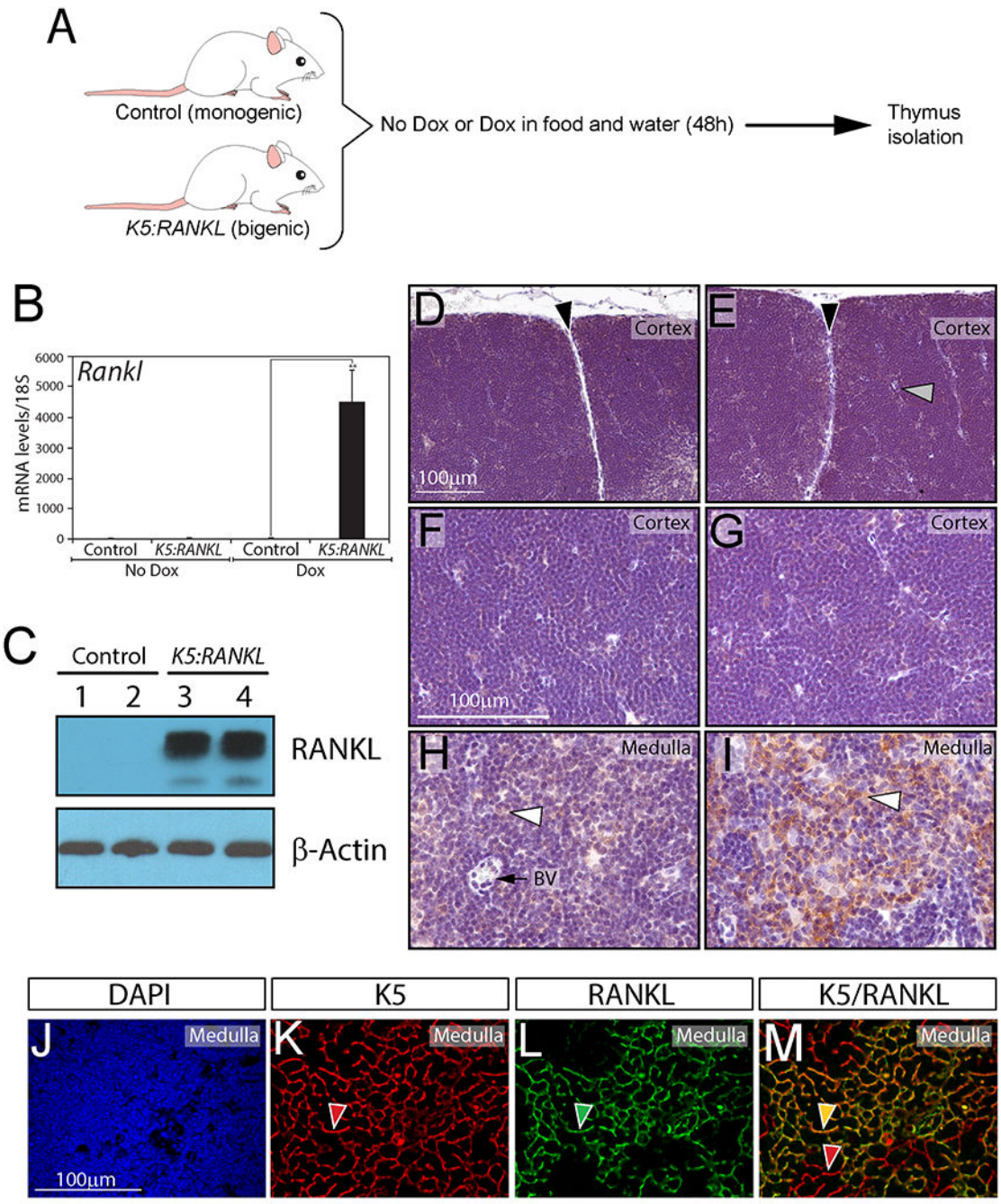

Fig. 1.

Acute doxycycline induction of RANKL in the thymus of the adult *K5: RANKL* bigenic mouse. (A) Controls (monogenic effector or responder transgenics) and *K5: RANKL* bigenics received regular food and water (no Dox) or food and water supplemented with Dox. Forty-eight hours following Dox-administration, control and *K5: RANKL* mice from all treatment groups were euthanized before thymi were removed for histological and molecular analysis. (B) Quantitative real-time PCR demonstrates that transgene derived *Rankl* (*Tnfsf 11*) transcript levels are significantly increased in the thymus of Dox-treated

K5: RANKL bigenics as compared with similarly treated control mice. Note: Thymic total RNA was pooled from five mice per genotype and treatment; the experiment was conducted in triplicate. (C) Western analysis shows the significant increase in thymic RANKL protein in the Dox-treated *K5: RANKL* bigenic group compared with the similarly treated control group (lanes 1-2 and 3-4 are duplicate lanes for control and *K5: RANKL* groups respectively); β-actin serves as a loading control. Note: each lane represents thymic protein pooled from five mice per genotype; the western result is representative of a triplicate. Note: In the absence of Dox, RANKL is not induced in the thymus of the *K5: RANKL* bigenic (see: Supplementary Fig. 1). (D) and (E) show the thymic cortex of adult control and *K5: RANKL* bigenic respectively (Dox-treated for 48 hours) following immunohistochemical staining for RANKL expression. Negligible levels of RANKL expression are detected in this thymic compartment (black and white arrowhead denote the interlobular septum and a pale reticular cell respectively). (F) and (G) are corresponding higher magnifications of regions within images shown in (D) and (E) respectively, which show low levels of endogenous RANKL expression. (H) and (I) show immunodetection (white arrowhead) of RANKL expression in the thymic medulla of the Dox-treated control and *K5: RANKL* bigenic respectively. Note the significant increase in RANKL expression levels in the *K5: RANKL* thymus (I) compared with the similarly treated control (H), which supports the western data shown in (C). Note: The relatively low level of endogenous RANKL in the medulla of the control thymus is not detected by western analysis (C) due to the significantly higher levels of transgene-derived RANKL in the *K5: RANKL* bigenic. Panel (J) shows a 48 hours Dox treated *K5: RANKL* bigenic thymic medulla section stained with DAPI. Panels (K) and (L) is the same section immunofluorescently stained for K5 (red) and RANKL (green) respectively. Panel (M) represents the superimposed images shown in (K and L) respectively. Red arrowhead shows location of K5 expression whereas green arrowhead shows location of RANKL expression; yellow arrowhead denotes areas of co-localization of K5 and RANKL expression (yellow/orange staining). Scale bars in (D) and (F) apply to (E) and (G-I) respectively. Scale bar in (J) applies to (K-M).

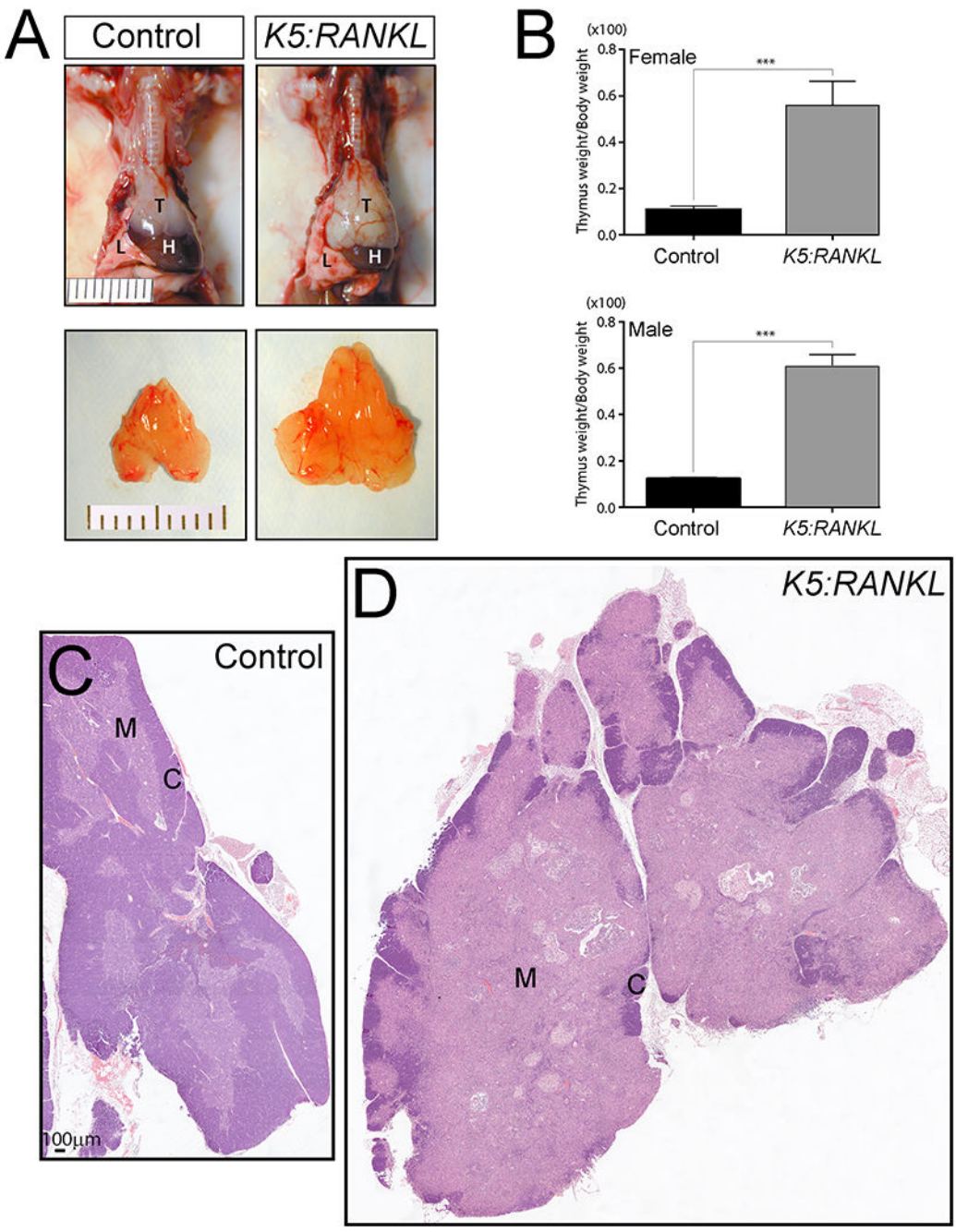

Fig. 2.

Significant enlargement of the thymic medulla in the *K5: RANKL* bigenic in response to prolonged Dox-administration. (A) Top panels show the thymus (T) *in situ* in the control and *K5: RANKL* bigenic following 10 days of Dox intake. Note the significant enlargement of the *K5: RANKL* bigenic thymus compared with the similarly treated control mouse; H and L denote heart and lung respectively. Bottom panels in (A) show the thymus dissected from the control (bottom left panel) and from the *K5: RANKL* bigenic (bottom right panel). The *K5: RANKL* thymus is significantly larger than the control; the ruler in the top and

bottom left panels apply to the top and bottom right panels respectively. (B) Top and bottom histograms display the mean average of thymus weight/body weight (± S.D.)) for control and *K5: RANKL* bigenic females and males respectively. For both sexes, the weight of the Dox-treated *K5: RANKL* thymus is at least three times that of the similarly treated control thymus. (C) Sagittal section of one lobe of the Dox treated control thymus showing the outer cortex (C) and inner medulla (M). (D) Sagittal section of both thymic lobes of the Dox treated *K5: RANKL* bigenic following staining with H&E. Note the clear expansion of the medullary region and a corresponding decrease in the cortical area. Scale bar in (C) applies to (D).

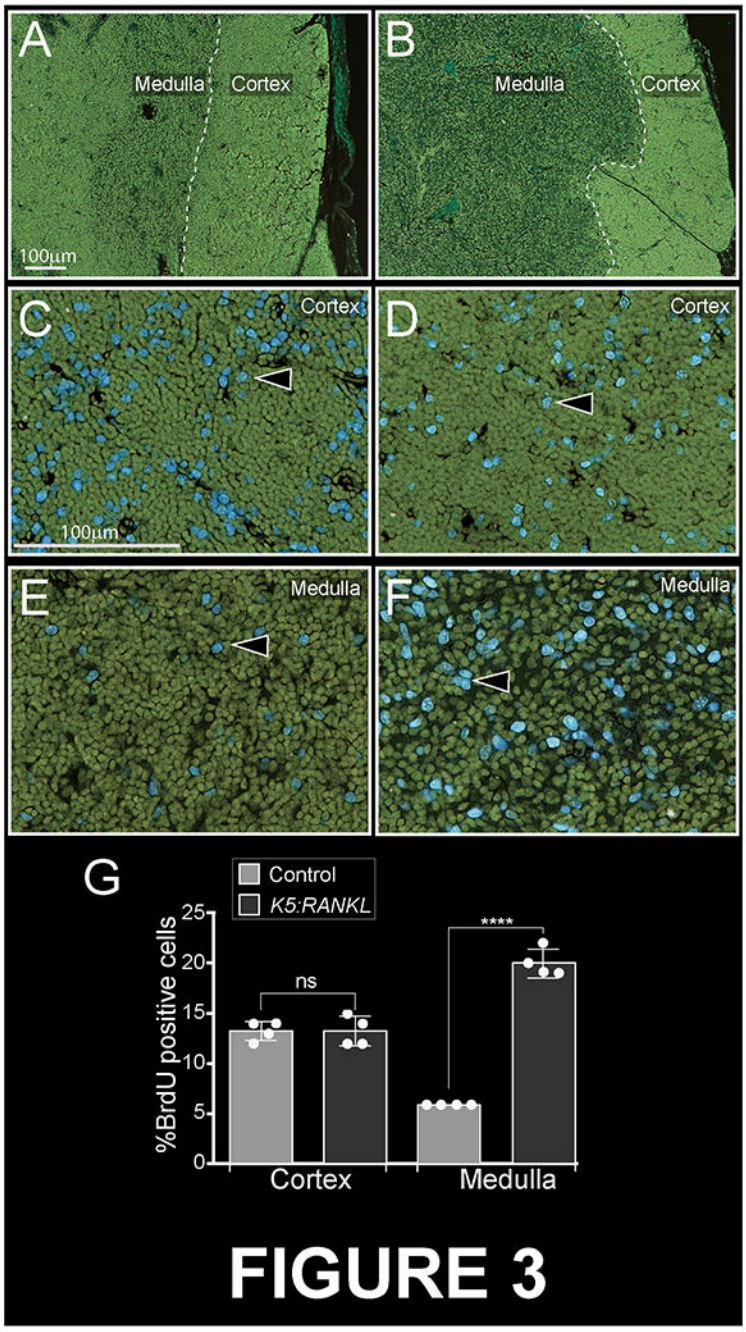

Fig. 3.

The thymic medulla of the ten day Dox-treated *K5-RANKL* bigenic shows a significant increase in cellular proliferation. For reference, panels (A) and (B) are H&E stained sections of the thymus from control and *K5: RANKL* bigenic mice following Dox-treatment for 10 days. The dashed line in each panel denotes the corticomedullary junction. (C) and (D) are high magnification images of the control and *K5: RANKL* thymic cortex respectively, each stained for BrdU incorporation. White arrowhead in each panel indicates a cortical cell immunopositive for BrdU incorporation. Panels (E) and (F) are high magnification

images of the control and *K5: RANKL* thymic medulla respectively that are stained for BrdU incorporation. White arrowhead in both panels highlights the location of a medullary cell immunopositive for BrdU incorporation. Note the significant increase in the number of BrdU positive cells in (F) compared to (E). Scale bar in (A) and (C) apply to (B) and (D-F) respectively. Panel (G) is a histogram quantitatively displaying the average percentage of BrdU positive cells in the cortical and medullary thymic compartments of similarly treated control and *K5: RANKL* mice (n= 4 per genotype).

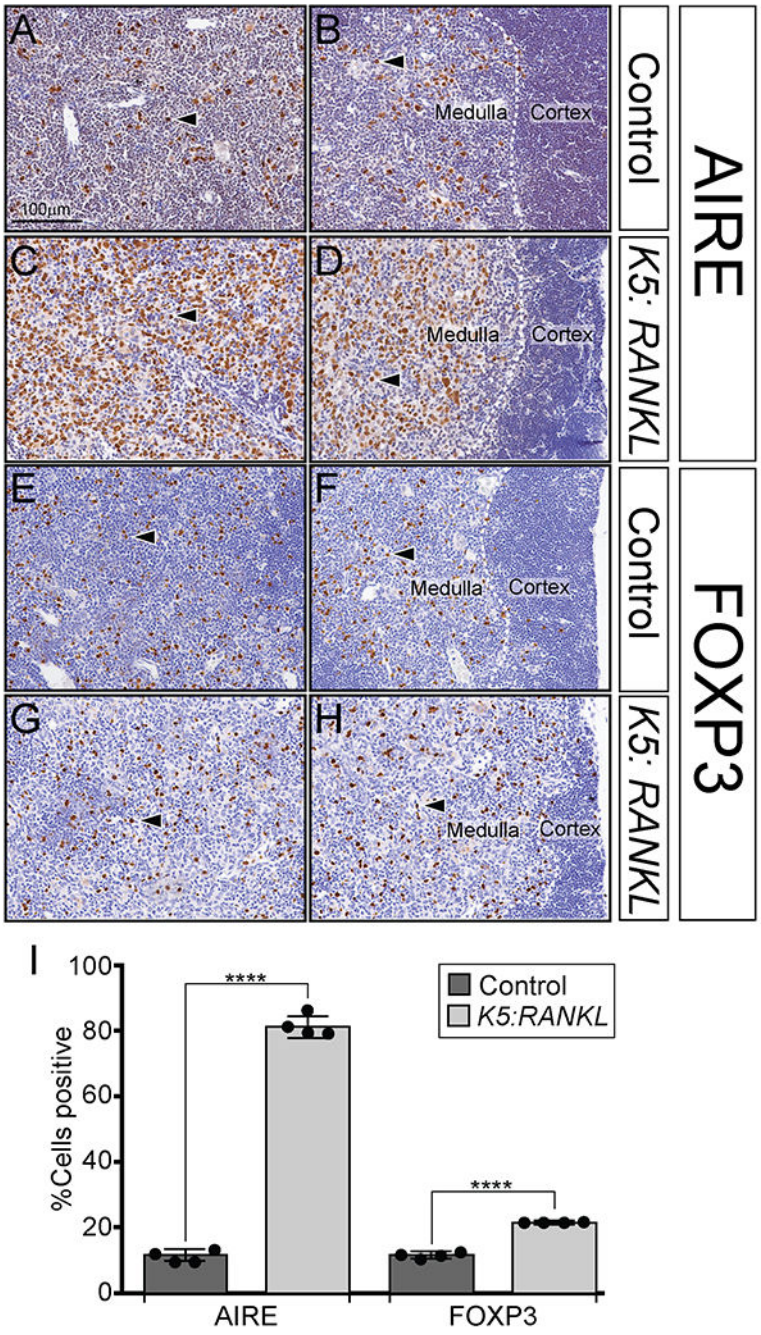

Fig. 4.

Increased numbers of AIRE and FOXP3 positive cells in the thymic medulla of the ten day Dox-treated *K5: RANKL* bigenic. (A) Section of thymic medulla of a Dox-treated monogenic control mouse stained for AIRE expression; black arrowhead indicates an mTEC immunopositive for AIRE expression. (B) Same immunostained section in (A) showing the corticomedullary junction (dashed white line). As expected, AIRE expression is restricted to the medulla compartment (black arrowhead). (C) Section of a similarly Dox-treated *K5: RANKL* thymic medulla stained for AIRE expression (black arrowhead). Note the marked

increase in the number of mTECs that are positive for AIRE expression (compare (C) with (A)). (D) Same immunostained tissue section in (C) showing the corticomedullary junction (dashed white line); black arrowhead indicates an AIRE positive mTEC. (E) Section of the thymic medulla of a Dox-treated monogenic control immunostained for FOXP3 expression (black arrowhead). (F) Same stained tissue section shown in (E) indicating the corticomedullary junction (white dashed line); black arrowhead points to a FOXP3 positive immune cell in the medulla. (G) Section of the thymic medulla of the *K5: RANKL* bigenic immunostained for FOXP3 expression (black arrowhead). Note the clear increase in the number of FOXP3 positive cells (compare (G) with (E)). (H) Same section in (G) showing the corticomedullary junction (dashed white line) and FOXP3 positive immune cells in the medulla (black arrowhead). Scale bar in (A) applies to all panels. Panel (I) shows a histogram quantitatively displaying the average percentage of thymic medulla cells that are positive for either AIRE or FOXP3 in the control and *K5: RANKL* bigenic following prolonged Dox-treatment (n= 4 per genotype).

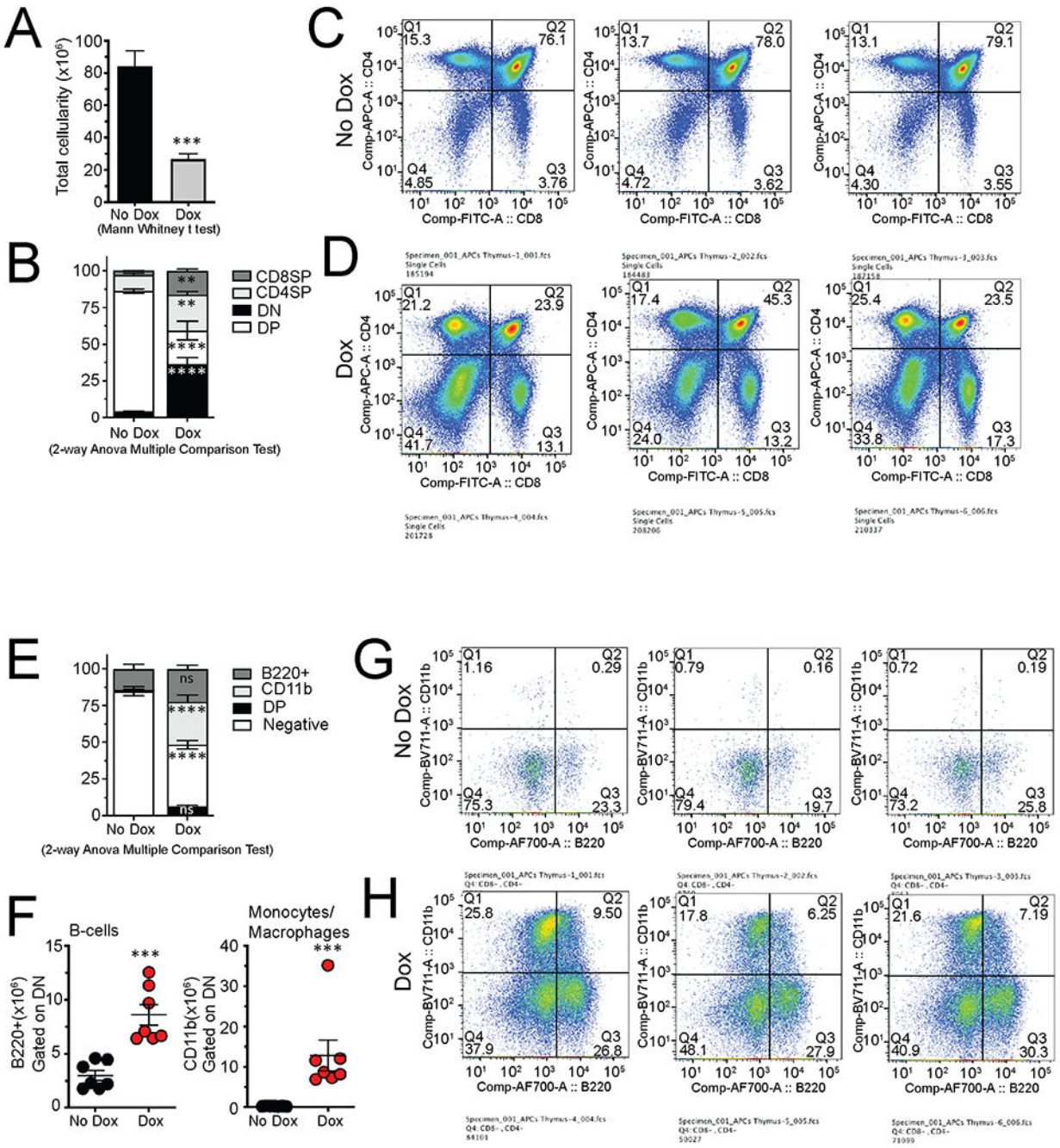

Fig. 5.

Flow cytometric analyses reveal significant alterations in the normal composition of thymocyte subtypes in the *K5: RANKL* bigenic thymus following prolonged Dox-administration. (A) Histogram shows mean total thymocyte cell numbers in the *K5: RANKL* thymus on regular chow and water (black bar) and following 10 days of Dox supplemented food and water (grey bar). Note that RANKL induction in the *K5: RANKL* thymus results in a significant decrease in total thymocyte numbers (n=3 mice per treatment). (B) The percentage of thymocyte subtypes (*i.e.* CD8 single positive (CD8+SP); CD4 single positive

(CD4+SP); CD8−/CD4− double negative (DN); and CD8+/CD4+ double positive (DP)) is significantly altered in the *K5: RANKL* thymus following 10-days of Dox-administration. Note the significant increase in the ratio of DN thymocytes and a corresponding decrease in the ratio of DP cells in Dox-treated *K5: RANKL* thymus. In particular, the percentage of CD8+SP and CD4+SP is significantly increased in the *K5: RANKL* thymus in response to Dox. Panels (C) and (D) logarithmically display the corresponding dot plots (Comp-APC-A:: CD4 stained cells (y-axis) *versus* Comp-FITC-A::CD8 stained cells (x-axis)) of thymocytes isolated from three individual *K5: RANKL* mice on regular food and water (No Dox) or three individual *K5: RANKL* mice on Dox supplemented food and water for 10-days (+Dox). Panel (E) shows a stacked bar graph displaying the percentage of B220+, CD11b+, B220+/CD11b+ (DP), and B220−/CD11b− (negative) immune cells in the thymus in the *K5: RANKL* without or with Dox supplemented food and water. (F) Number of B cells (left graph) and monocytes/macrophages (right graph) within the DN population. Note the significant increase in B-cell (B220+) and monocytes/macrophages (CD11b+) cell numbers in the thymus of Dox-treated *K5: RANKL* bigenic mice. Panels (G) and (H) show the thymic flow dot plots (Comp-BV711-A:: CD11b stained cells (y-axis) *versus* Comp-AF700-A::B220 stained cells (x-axis)) of *K5: RANKL* mice on regular food and water or Dox supplemented food and water respectively (three *K5: RANKL* mice without (No Dox) or with Dox (Dox)).

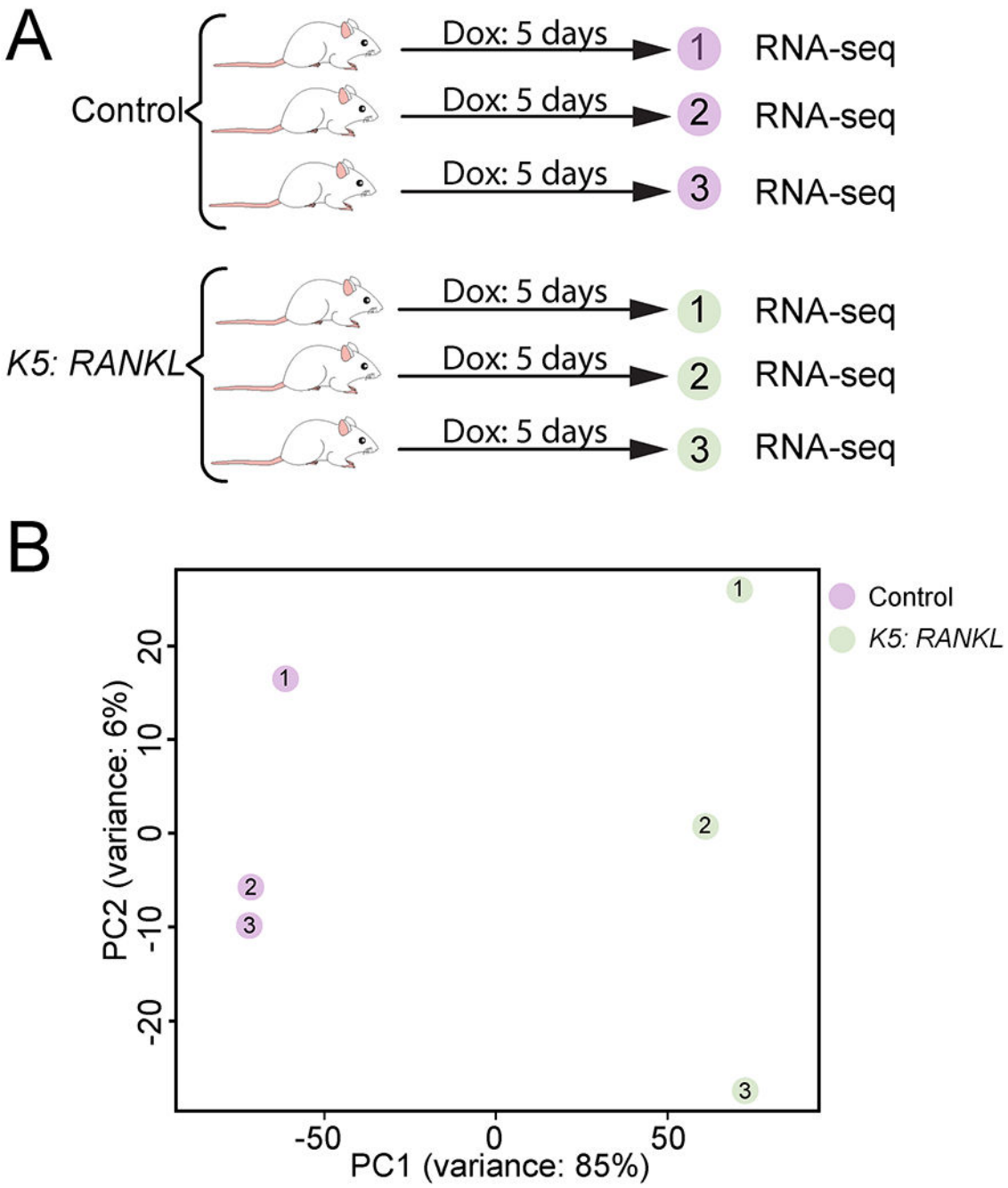

Fig. 6.

The experimental design of the thymic RNA-seq experiment. (A) Adult (9-week old) monogenic controls and *K5: RANKL* bigenics (triplicates per genotype) received Dox-supplemented food and water for 5-days before whole thymi were removed for RNA preparation and subsequent RNA-seq analysis. (B) Using the raw gene count data (fragments per kilobase of transcript per million (FPKM) values), principal component analysis was performed with the R function prcomp package (https://cran.r-project.org). Principal

component analysis demonstrated that respective triplicates for the control and *K5: RANKL* groups clustered separately.

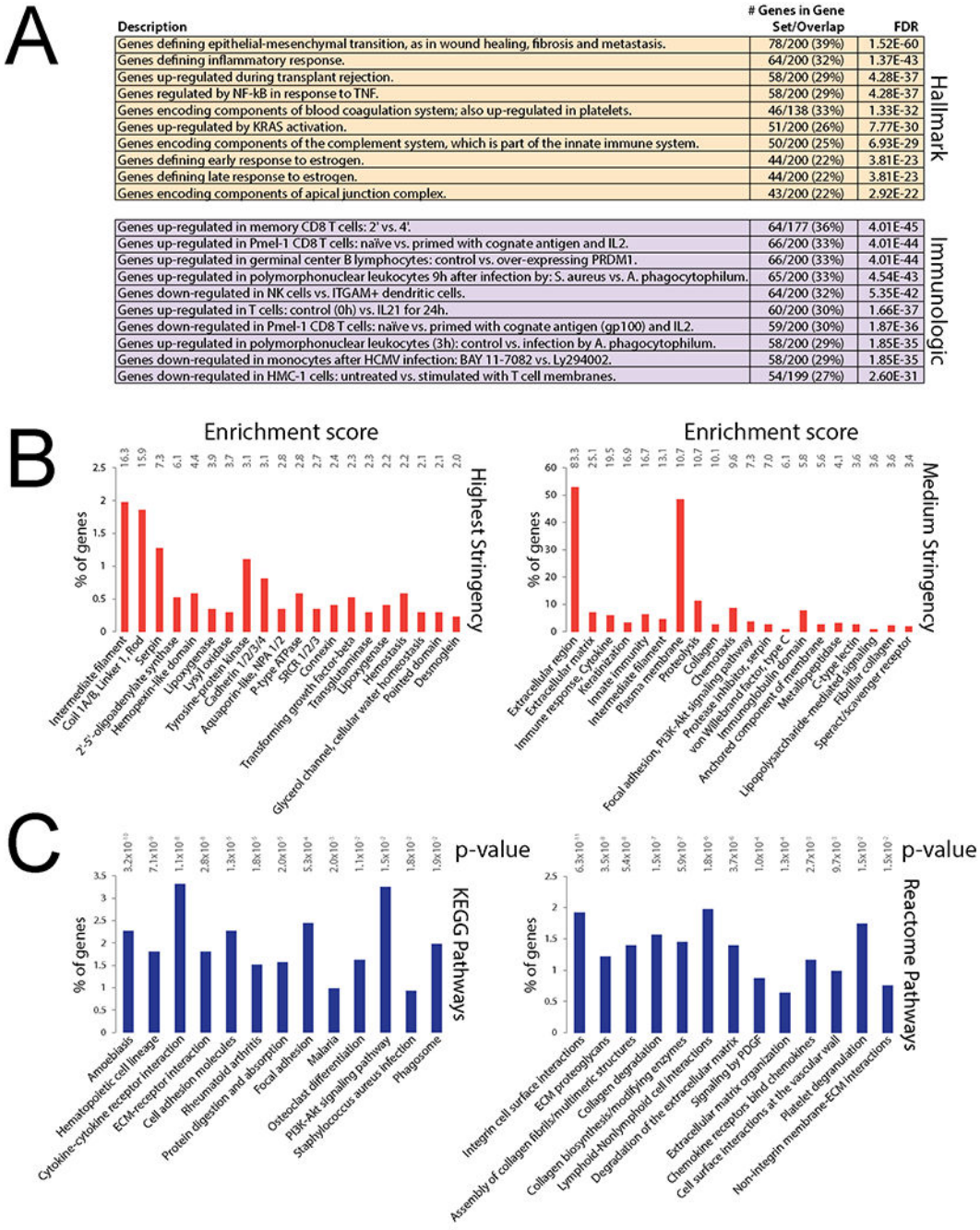

Fig. 7.

Bioinformatic analysis of differentially expressed genes between Dox-treated *K5: RANKL* and similarly treated monogenic control thymic tissue. (A) Gene Set Enrichment Analysis of genes with significant expression changes—(|FC|>5, FDR < 0.05, and sum of mean counts >100)—in the thymus of *K5: RANKL* mice compared with monogenic controls. The differentially expressed gene set between the two groups was compared to the Hallmark and Immune Collection of the Molecular Signatures Database. (B) Summaries of DAVID Functional Annotation Clustering analysis of the differentially expressed gene set after

applying two levels of stringency (the highest (|FC|>5) and medium levels (|FC|>2)). (C) DAVID pathway analysis of the differentially expressed gene set run against the KEGG and Reactome pathway databases.

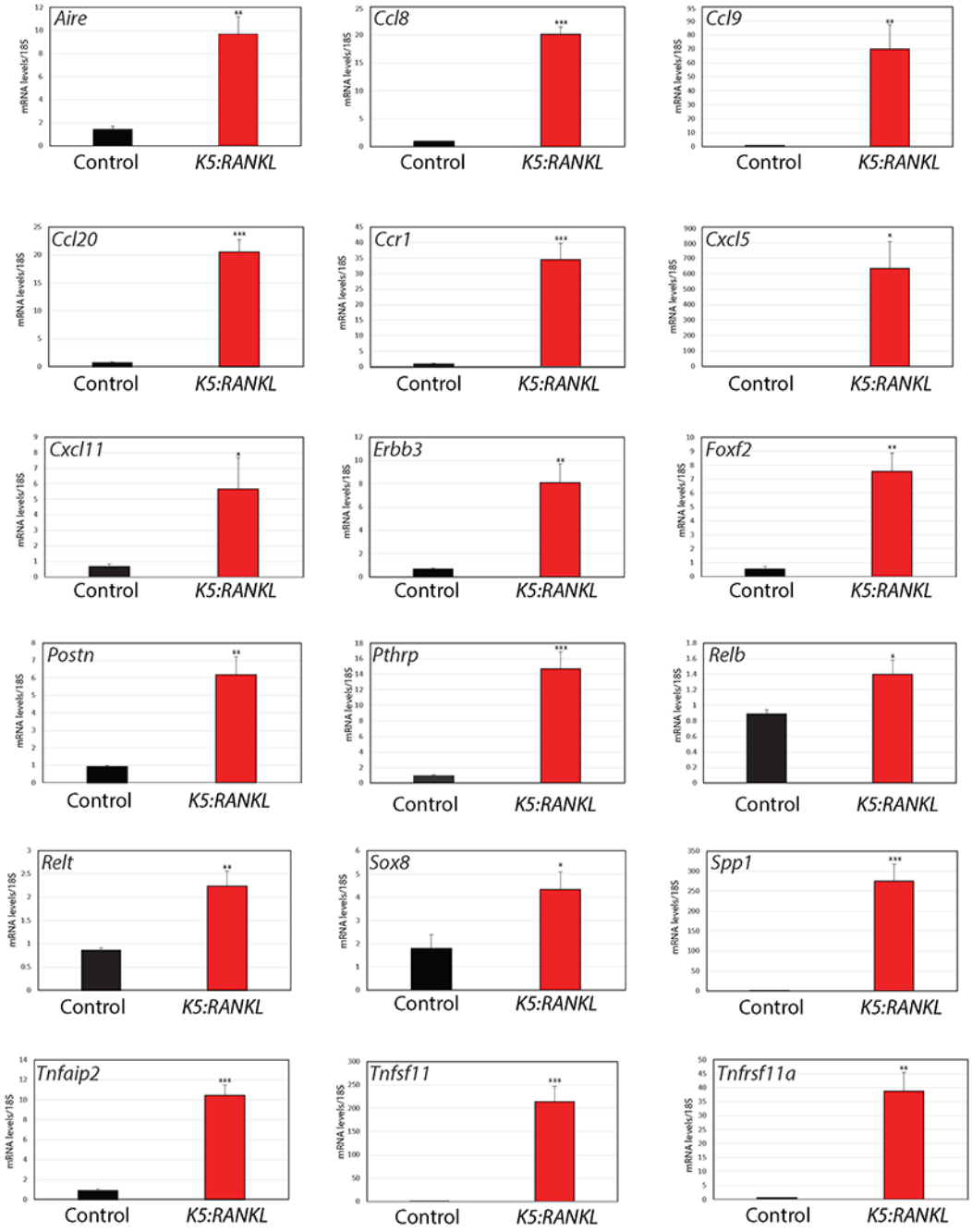

Fig. 8.

Immune, NFκB, TNF and epithelial cell signaling are significantly enriched in the *K5: RANKL* thymic transcriptome. In addition to *Aire*, quantitative real-time PCR reveals that the transcript levels of members of the chemokine/chemokine receptor family (*i.e.* chemokine (C-C motif) ligand 8 (*Ccl8*); *Ccl9*; *Ccl20*, and C-C chemokine receptor type 1 (*Ccr1*)) are significantly expressed in the Dox-treated *K5: RANKL* thymus. The transcript levels of C-X-C motif chemokine 5 (*Cxcl5*) and *Cxcl11* are also markedly elevated in the *K5: RANKL* thymic transcriptome. Factors involved in epithelial cell signaling in general

and TNF signaling in particular such as *epidermal growth factor receptor b3* (*Erbb3*); *forkhead box F2* (*Foxf2*); *periostin* (*Postn*); *parathyroid hormone-related (or like) hormone (Pthr(I)h)*; *RelB proto-oncogene*; *Relt* (TNF receptor superfamily member 19L); *Sox8* (SRY-related HMG-box family transcription factor); secreted protein 1 (*Spp1*); (TNF alpha induced protein 2 (*Tnfaip2*); *Tnfsf11* (*RANKL*); and *TNF receptor superfamily member 11a* (*Tnfrsf11a* (*RANK*)) are highly expressed in Dox-treated *K5: RANKL* thymic tissue. Data are presented as the average expression fold change relative to control group ± standard deviation (n=4 mice per monogenic control and *K5: RANKL* bigenic groups).

Table 1

List of murine Taqman expression assays used in these studies.

Gene symbol	Entrez Gene ID	Catalog number
Aire	11634	Mm00477450_g1
Ccl8	20307	Mm01297183_m1
Ccl9	20308	Mm00441260_m1
Ccl20	20297	Mm01268754_m1
Ccr1	12768	Mm00438260_s1
Cxcl5	20311	Mm00436451_g1
Cxcl11	56066	Mm00444662_m1
Erbb3	13867	Mm01159999_m1
Postn	50706	Mm01284919_m1
Pthrp/Pthlh	19227	Mm00436057_m1
Relb	19698	Mm00485664_m1
Relt	320100	Mm00723872_m1
Sox8	20681	Mm00803422_m1
Spp1	20750	Mm00436767_m1
Tnfaip2	21928	Mm00447578_m1
Tnfrsf11 (Rankl)	21943	Mm00441906_m1
Tnfrsf11a (Rank)	21934	Mm01286487_m1
18S rRNA	Thermo Fisher Scientific Inc.: 4352930E	

Table 2

Top 50 genes upregulated in the *K5: RANKL* thymus.

GENE SYMBOL	GENE ID	GENE NAME	K5:RANKL/CONTROL
Cxcl5	20311	chemokine (C-X-C motif) ligand 5	1414.2
Arg1	11846	arginase, liver	948.1
Sprr2g	20761	small proline-rich protein 2G	670.2
Krt6b	16688	keratin 6B	626.9
Tmprss11g	320454	transmembrane protease, serine 11g	533.6
Sprr2d	20758	small proline-rich protein 2D	499.1
Cwh43	231293	cell wall biogenesis 43 C-terminal homolog	487.8
Tnfsf11	**21943**	**tumor necrosis factor (ligand) superfamily, member 11**	**449.9**
Csta1	209294	cystatin A1	449.8
Chil4	104183	chitinase-like 4	440.9
Spp1	20750	secreted phosphoprotein 1	436.8
Sprr2h	20762	small proline-rich protein 2H	338.4
Chil3	12655	chitinase-like 3	327.1
Sprr2e	20759	small proline-rich protein 2E	312.7
Gm5483	433016	predicted gene 5483	304.7
Gm10872			298.4
Il19	329244	interleukin 19	285.0
Mmp13	17386	matrix metallopeptidase 13	284.4
Sprr2b	20756	small proline-rich protein 2B	284.3
Trem1	58217	triggering receptor expressed on myeloid cells 1	274.4
Slfn4	20558	schlafen 4	260.7
Sprr2i	20763	small proline-rich protein 2I	244.5
Il1f9	215257	interleukin 1 family, member 9	240.4
Il24	93672	interleukin 24	231.4
Defb3	27358	defensin beta 3	227.4
BC117090	100038854	cDNA sequence BC1179090	225.7
Sprr2f	20760	small proline-rich protein 2F	225.6
Defb14	244332	defensin beta 14	214.8
Lce3a	545548	late cornified envelope 3A	211.1
Lcn2	16819	lipocalin 2	194.8
BC100530	100034684	cDNA sequence BC100530	192.6
Uox	22262	urate oxidase	187.8
Lce3f	69520	late cornified envelope 3F	184.1
Cxcr2	12765	chemokine (C-X-C motif) receptor 2	184.0
F7	14068	coagulation factor VII	177.7
Slc28a3	114304	solute carrier family 28 (sodium-coupled nucleoside transporter), member 3	166.5
Ltf	17002	lactotransferrin	164.2

GENE SYMBOL	GENE ID	GENE NAME	K5:RANKL/CONTROL
Nlrp12	378425	NLR family, pyrin domain containing 12	157.7
Cnfn	72383	cornifelin	157.6
Krt6a	16687	keratin 6A	156.0
Mmp12	17381	matrix metallopeptidase 12	153.5
Rnase2b	54159	ribonuclease, RNase A family, 2B (liver, eosinophil-derived neurotoxin)	143.9
Sprr1b	20754	small proline-rich protein 1B	140.7
4732456N10Rik	239673	RIKEN cDNA 4732456N10 gene	137.0
Olr1	108078	oxidized low density lipoprotein (lectin-like) receptor 1	135.3
S100a7a	381493	S100 calcium binding protein A7A	134.4
Stfa2l1	268885	stefin A2 like 1	132.7
Prss27	213171	protease, serine 27	132.1
Cxcl2	20310	chemokine (C-X-C motif) ligand 2	131.4
Sprr2j-ps	20764	small proline-rich protein 2J, pseudogene	128.9

Table 3

Top 50 genes downregulated in the *K5: RANKL* thymus.

GENE SYMBOL	GENE ID	GENE NAME	K5:RANKL/CONTROL
Psmb11	73902	proteasome (prosome, macropain) subunit, beta type, 11	−39.0
Gm3716	100042198	predicted gene 3716	−32.2
Ptcra	19208	pre T cell antigen receptor alpha	−31.2
C2cd4d	271944	C2 calcium-dependent domain containing 4D	−28.6
Themis	210757	thymocyte selection associated	−27.1
Gm6623	625785	akirin 1 pseudogene	−25.0
1700097N02Rik	67522	RIKEN cDNA 1700097N02 gene	−24.4
Usp44	327799	ubiquitin specific peptidase 44	−23.9
H2-T3	15043	histocompatibility 2, T region locus 3	−23.3
Rag1	19373	recombination activating gene 1	−21.7
Trat1	77647	T cell receptor associated transmembrane adaptor 1	−21.3
Dntt	21673	deoxynucleotidyltransferase, terminal	−20.7
Slc16a5	217316	solute carrier family 16 (monocarboxylic acid transporters), member 5	−20.6
Gm20098	100504169	predicted gene, 20098	−20.3
Insl5	23919	insulin-like 5	−20.3
Arpp21	74100	cyclic AMP-regulated phosphoprotein, 21	−20.1
Cnga1	12788	cyclic nucleotide gated channel alpha 1	−19.5
Tctex1d1	67344	Tctex1 domain containing 1	−17.5
H2-Q1	15006	histocompatibility 2, Q region locus 1	−17.4
Sh2d1a	20400	SH2 domain containing 1A	−17.3
Ccr9	12769	chemokine (C-C motif) receptor 9	−17.0
Wdr78	242584	WD repeat domain 78	−16.9
A930003A15Rik	68162	RIKEN cDNA A930003A15 gene	−16.7
Prss16	54373	protease, serine 16 (thymus)	−16.1
Chrna9	231252	cholinergic receptor, nicotinic, alpha polypeptide 9	−15.8
Rorc	19885	RAR-related orphan receptor gamma	−15.7
2310065F04Rik	74184	RIKEN cDNA 2310065F04 gene	−15.5
BB031773	100473	expressed sequence BB031773	−15.5
Cd8b1	12526	CD8 antigen, beta chain 1	−15.4
Crip3	114570	cysteine-rich protein 3	−15.1
Vmn2r84	625068	vomeronasal 2, receptor 84	−15.1
Gm12709	100504717	predicted gene 12709	−15.0
Gm4371	100043335	eukaryotic translation initiation factor 3, subunit I pseudogene	−14.7
H2-Q2	15013	histocompatibility 2, Q region locus 2	−14.7
Nwd1	319555	NACHT and WD repeat domain containing 1	−14.4
Cdca7	66953	cell division cycle associated 7	−14.3
Ankmy1	241158	ankyrin repeat and MYND domain containing 1	−14.3

GENE SYMBOL	GENE ID	GENE NAME	K5:RANKL/CONTROL
Ccl25	20300	chemokine (C-C motif) ligand 25	−14.2
4933409K07Rik	108816	RIKEN cDNA 4933409K07 gene	−14.2
Tcf7	21414	transcription factor 7, T cell specific	−14.1
Mns1	17427	meiosis-specific nuclear structural protein 1	−13.8
Nsg2	18197	neuron specific gene family member 2	−13.8
Xrra1	446101	X-ray radiation resistance associated 1	−13.6
Satb1	20230	special AT-rich sequence binding protein 1	−13.4
2610318N02Rik	70458	RIKEN cDNA 2610318N02 gene	−13.2
Aox2	213043	aldehyde oxidase 2	−13.1
Cd8a	12525	CD8 antigen, alpha chain	−13.0
Nyap1	243300	neuronal tyrosine-phosphorylated phosphoinositide 3-kinase adaptor 1	−12.8
Rag2	19374	recombination activating gene 2	−12.7
E2f2	242705	E2F transcription factor 2	−12.6
Arsi	545260	arylsulfatase i	−12.6